Enhanced Direct Air Capture by Uranyl Superoxide: A Comprehensive Study of the Carbonation Reaction of Uranyl Peroxide Complexes

Sarah K. Scherrer [a], Tori Forbes [a,*]

[a] Department of Chemistry, University of Iowa, Iowa City, Iowa 52242, United States

* Correspondence to: tori-forbes@uiowa.edu

Table of Contents

Carbonation Reaction Kinetic Modelling

Reaction Apparatus

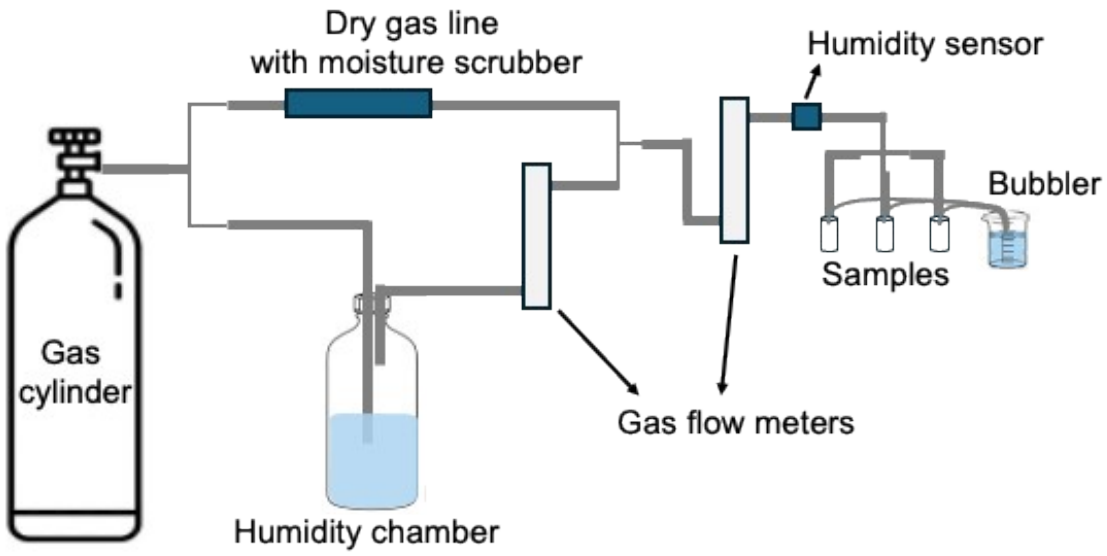

Figure S1. Diagram of the custom-built apparatus utilized for the flow-through experiments.

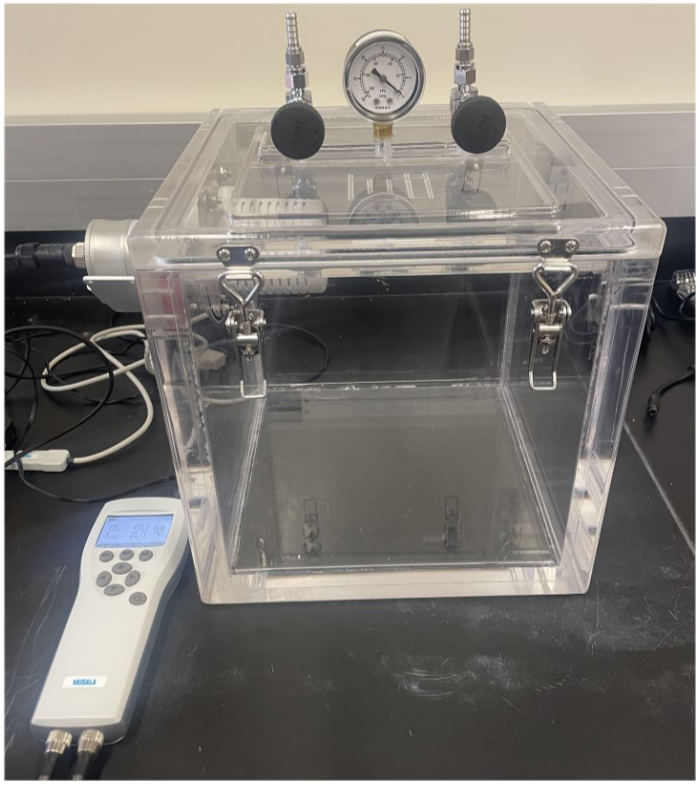

Figure S2. Image of the air-tight apparatus equipped with a CO_2 sensor used for kinetic studies.

Characterization of the pure materials

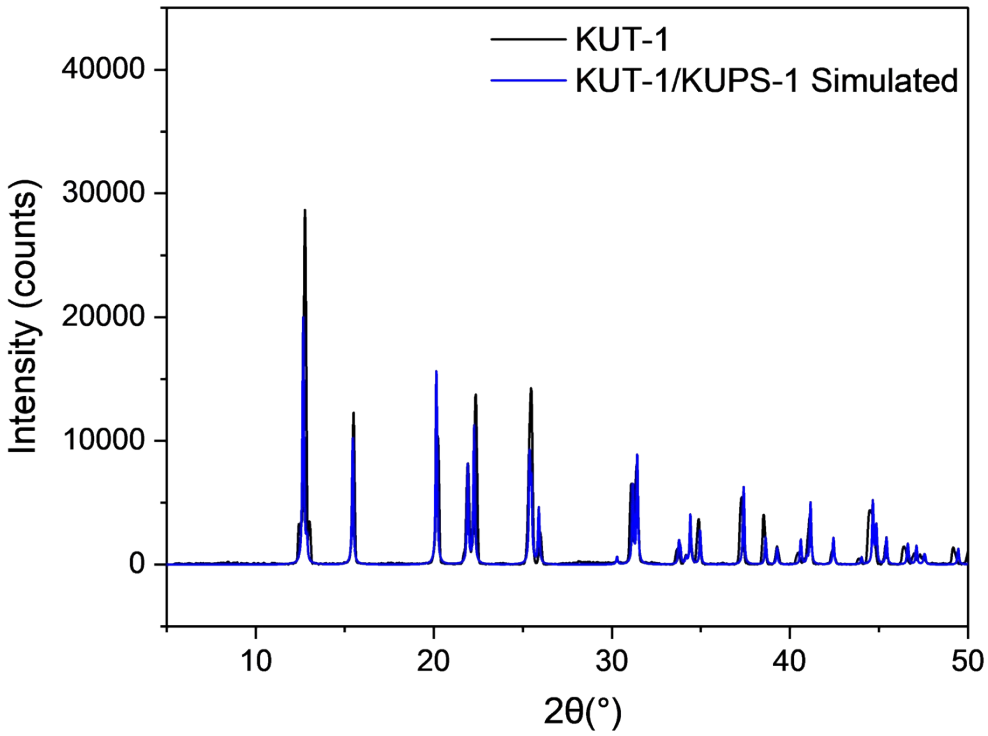

Figure S3. PXRD of the pristine KUT-1 material (black) and the simulated KUT-1 pattern (blue).

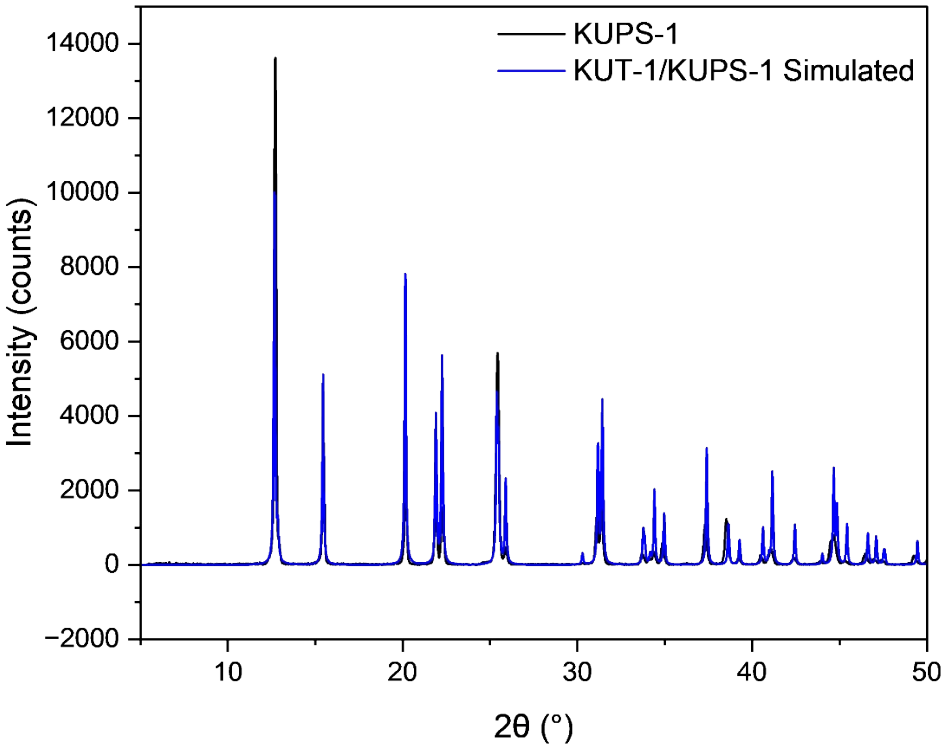

Figure S4. PXRD of the pristine KUPS-1 material (black) and the simulated KUPS-1 pattern (blue).

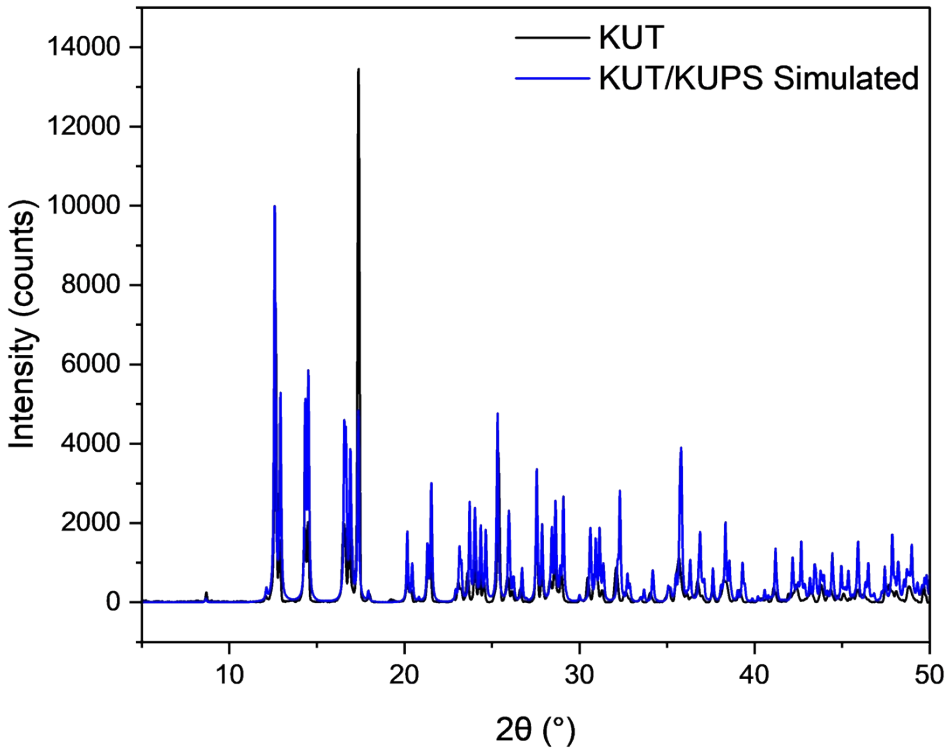

Figure S5. PXRD of the pristine KUT material (black) and the simulated KUT pattern (blue).

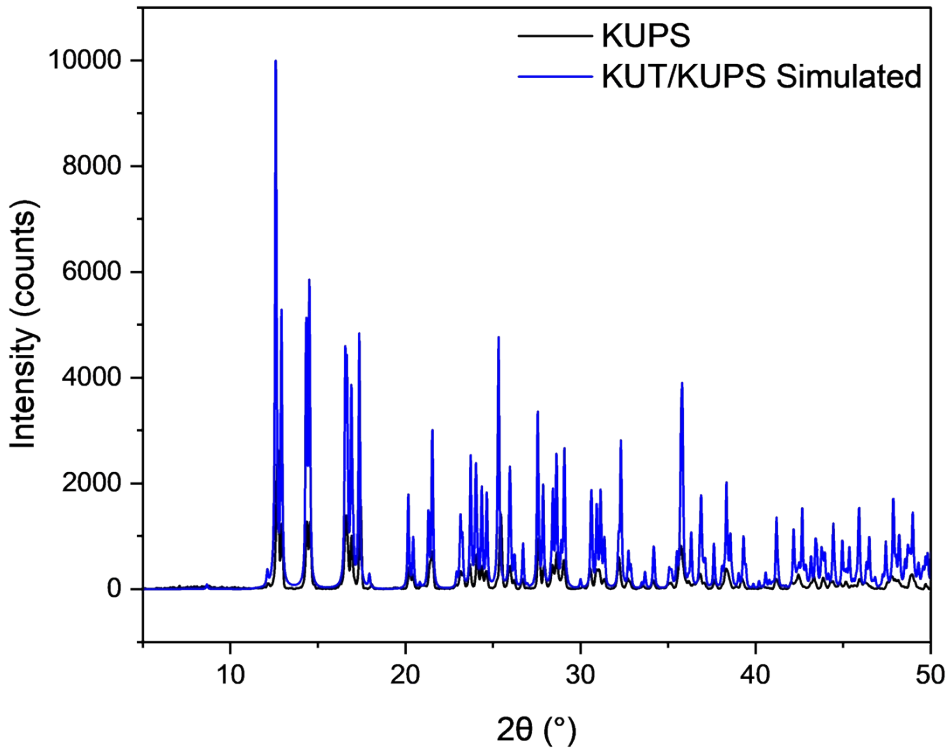

Figure S6. PXRD of the pristine KUPS material (black) and the simulated KUPS pattern (blue).

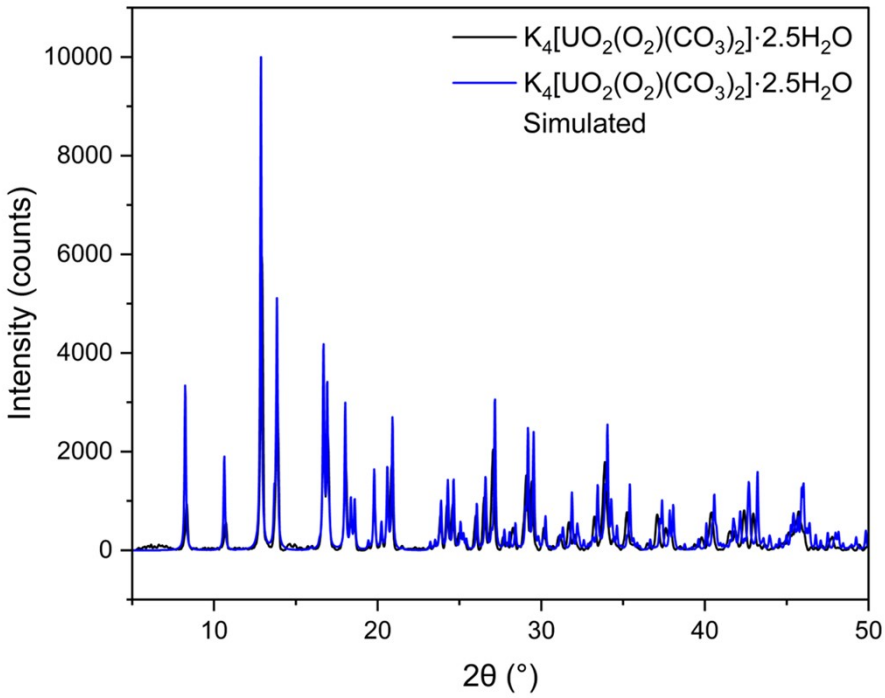

Figure S7. PXRD of the U(VI) peroxo-carbonate compound (black) and the pattern simulated from the structural characterization by Goff *et al*. (blue).

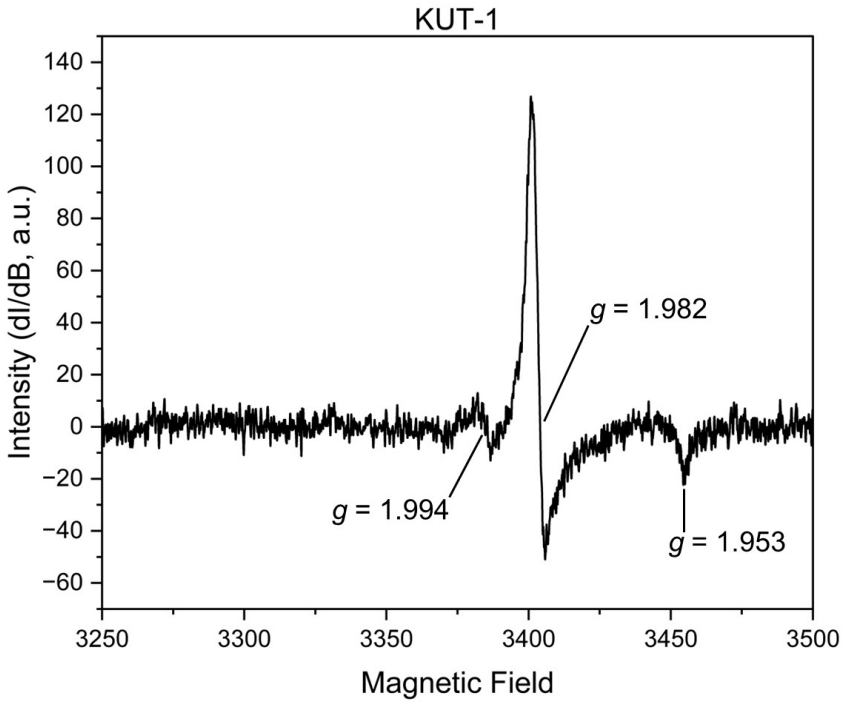

Figure S8. EPR spectrum of the KUT-1 material. Features at *g* = 1.994, 1.982, and 1.953 correspond to a Cr(V) peroxide trace contaminant.

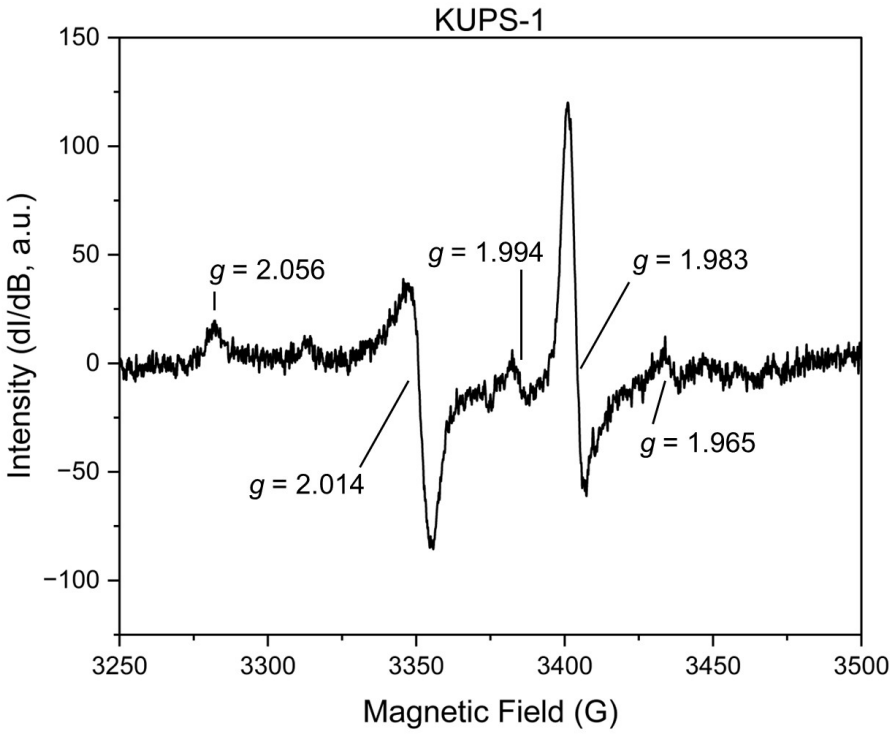

Figure S9. EPR spectrum of the KUPS-1 material. Features at g = 1.994, 1.982, and 1.965 correspond to a Cr(V) peroxide trace contaminant. Additional signatures ($g_{\parallel}$ = 2.056, $g_{\perp}$ = 2.014) have been identified as superoxide complexed to the U(VI) cation.

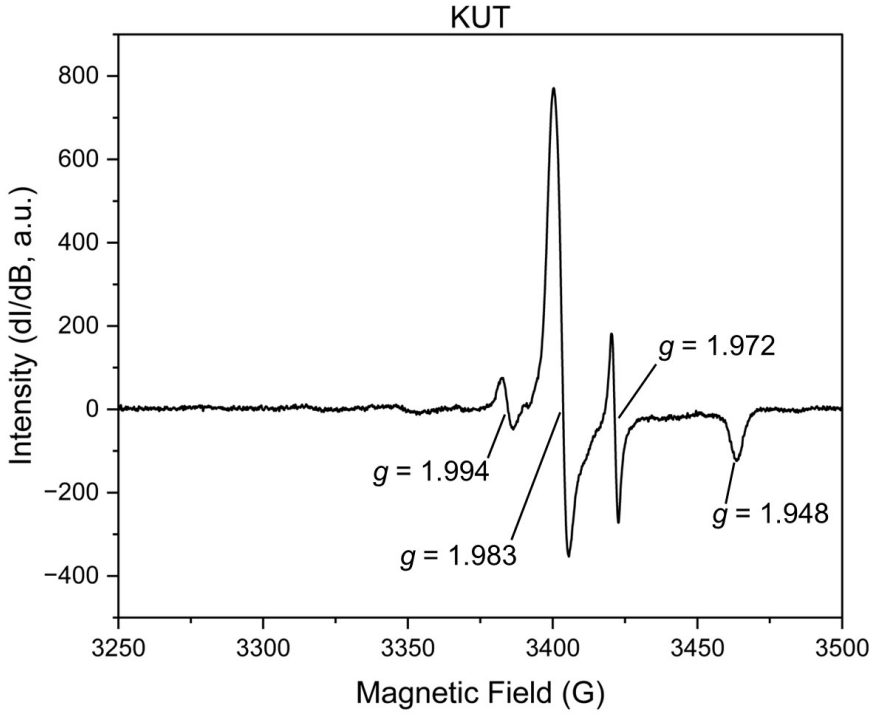

Figure S10. EPR spectrum of the KUT material. Features at g = 1.994, 1.983, 1.972 and 1.948 correspond to a Cr(V) peroxide trace contaminant.

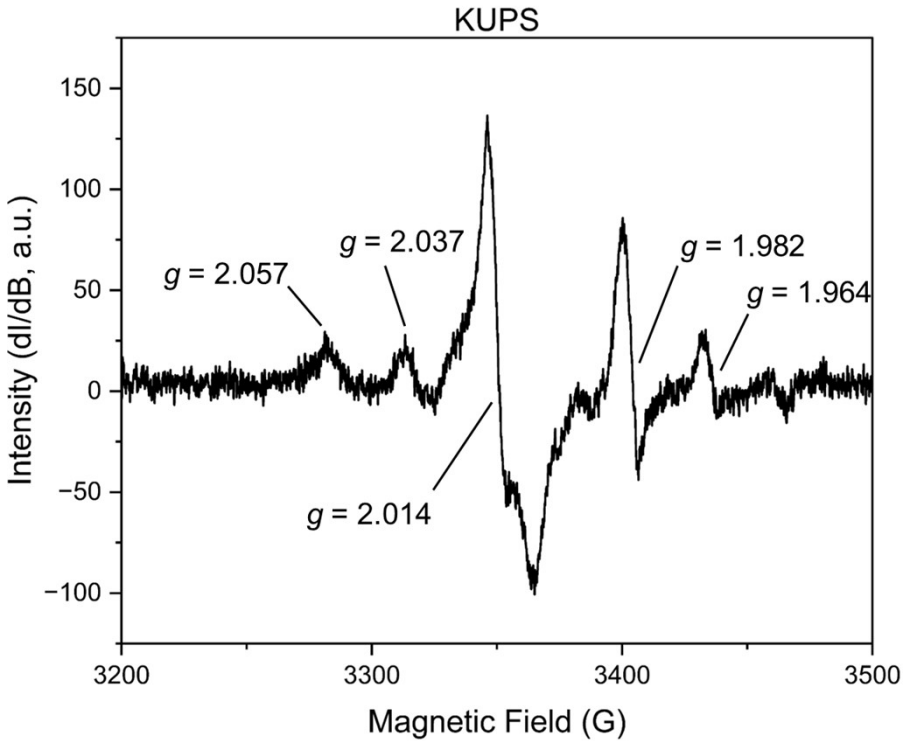

Figure S11. EPR spectrum of the KUPS material. Features at g = 1.982 and 1.964 correspond to a Cr(V) peroxide trace contaminant. Additional signatures ($g_{\parallel}$ = 2.057/2.037, $g_{\perp}$ = 2.014) correspond to superoxide complexed to the U(VI) cation.

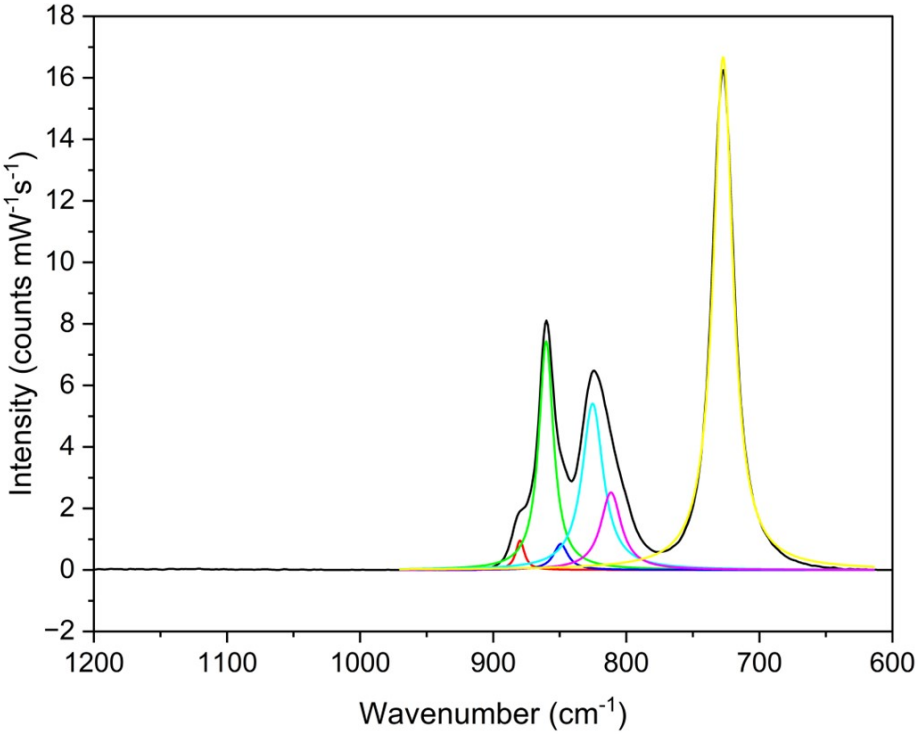

Figure S12. Fitted Raman spectrum of KUT-1 in the spectral window of interest (χ^2 = 0.05; R^2 = 0.999).

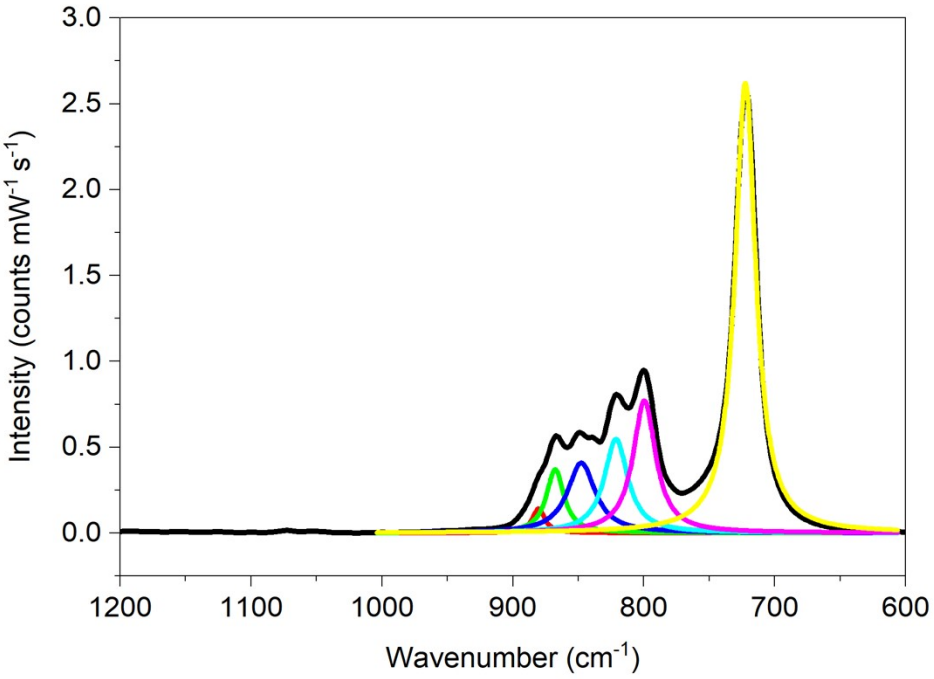

Figure S13. Fitted Raman spectrum of KUPS-1 in the spectral window of interest (χ^2 = 7.87 x 10^{-4}; R^2 = 0.997).

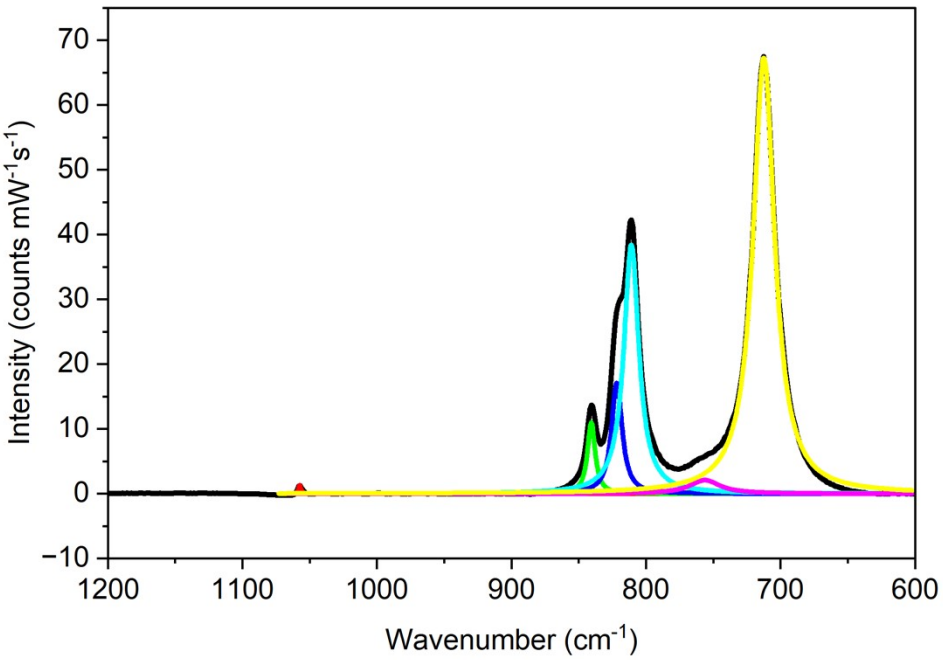

Figure S14. Fitted Raman spectrum of KUT in the spectral window of interest (χ^2 = 0.28; R^2 = 0.998). Additional feature at 1057 cm^{-1} indicates a small amount of carbonate on the surface of the sample.

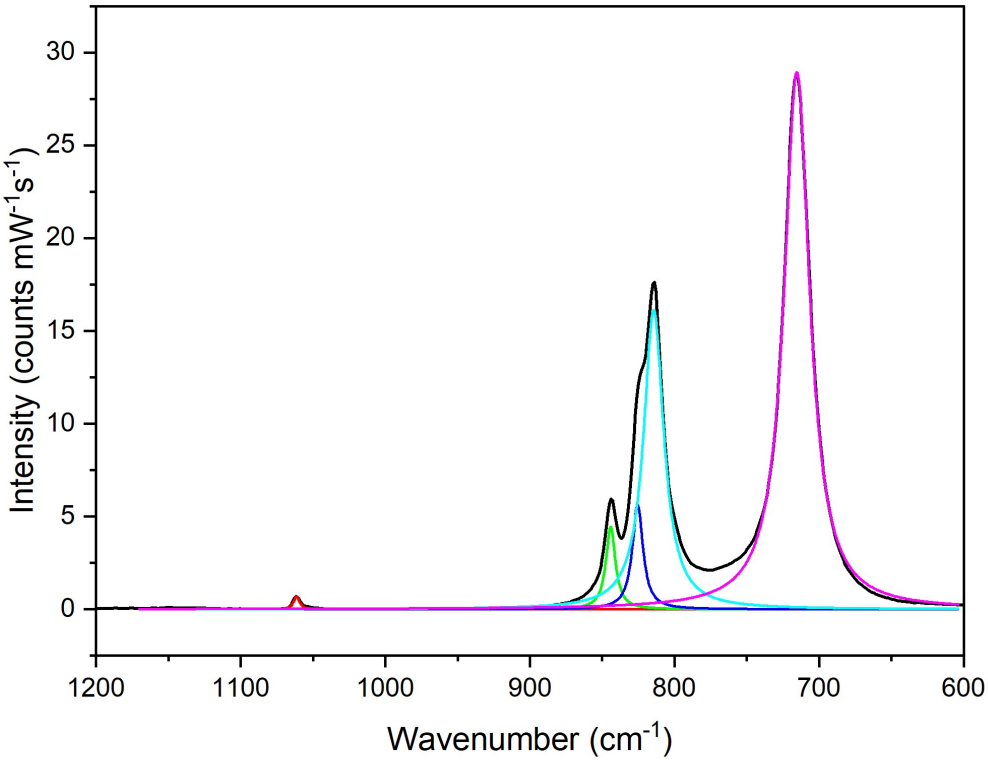

Figure S15. Fitted Raman spectrum of KUPS in the spectral window of interest ($\chi^2 = 0.041$; $R^2 = 0.999$). Additional feature at 1061 cm^{-1} indicates a small amount of carbonate on the surface of the sample.

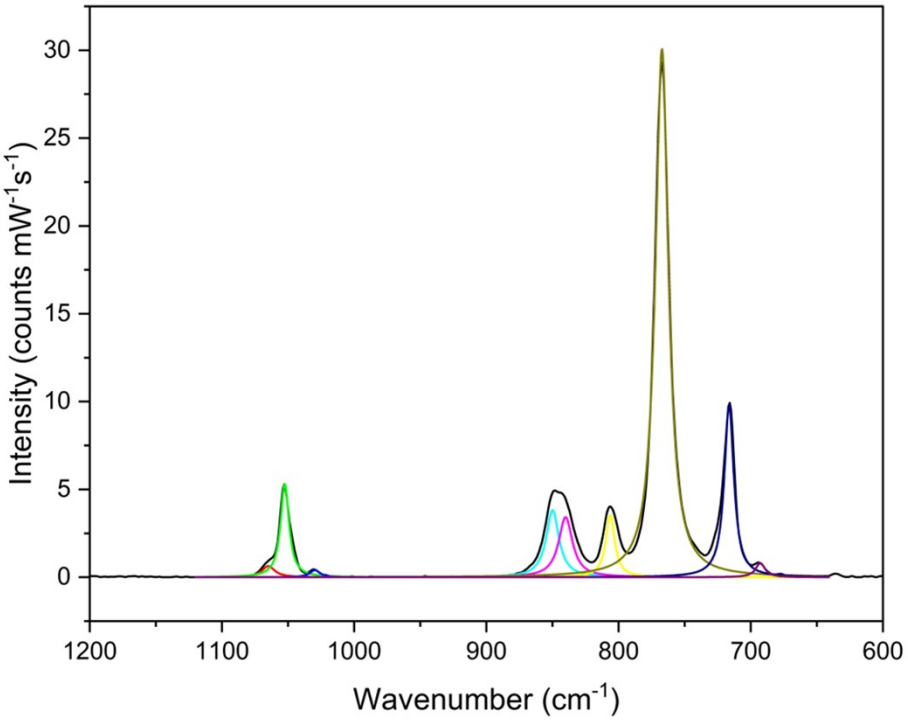

Figure S16. Fitted Raman spectrum of $K_4(UO_2(O_2)(CO_3)_2 \bullet 2.5H_2O$ in the spectral window of interest of ($\chi^2 = 0.08$; $R^2 = 0.999$).

Elemental Analysis of Carbonation Reactions

Table S1. Average carbon content for each material as synthesized, after reaction with pure CO_2 and compressed air at different relative humidity values, and after the kinetics batch studies.

Sample		% C	mol C/mol U
KUT-1		0.095 ± 0.004	0.057 ± 0.002
CO_2	15% RH	0.207 ± 0.129	0.125 ± 0.078
	45% RH	4.800 ± 0.065	2.896 ± 0.039
	70% RH	4.290 ± 0.040	2.588 ± 0.024
Compressed Air	15% RH	0.117 ± 0.031	0.070 ± 0.019
	45% RH	0.240 ± 0.152	0.145 ± 0.092
	70% RH	0.287 ± 0.076	0.173 ± 0.046
Kinetics Study		3.345 ± 0.201	2.018 ±0.121
KUPS-1		0.087 ± 0.029	0.052 ± 0.017
CO_2	15% RH	0.130 ± 0.081	0.078 ± 0.049
	45% RH	3.223 ± 0.416	1.945 ± 0.251
	70% RH	2.978 ± 0.040	1.797 ± 0.024
Compressed Air	15% RH	0.167 ± 0.017	0.101 ± 0.010
	45% RH	0.276 ± 0.022	0.167 ± 0.014
	70% RH	0.157 ± 0.052	0.095 ± 0.032
Kinetics Study		3.883 ± 0.048	2.342 ± 0.029
KUT		0.047 ± 0.082	0.028 ± 0.049
CO_2	15% RH	1.067 ± 0.052	0.643 ± 0.032
	45% RH	4.397 ± 0.039	2.652 ± 0.023
	70% RH	4.380 ± 0.020	2.642 ± 0.012
Compressed Air	15% RH	0.497 ± 0.024	0.300 ± 0.014
	45% RH	0.427 ± 0.054	0.257 ± 0.033
	70% RH	0.450 ± 0.010	0.271 ± 0.006
Kinetics Study		3.028 ± 0.447	1.827 ± 0.270
KUPS		0.045 ± 0.003	0.027± 0.002
CO_2	15% RH	0.475 ± 0.035	0.287 ± 0.021
	45% RH	4.247 ± 0.009	2.562 ± 0.006
	70% RH	3.093 ± 0.086	1.866 ± 0.052
Compressed Air	15% RH	0.435 ± 0.015	0.262 ± 0.009
	45% RH	0.415 ± 0.005	0.250 ± 0.003
	70% RH	0.440 ± 0.065	0.265 ± 0.039
Kinetics Study		3.460 ± 0.010	2.087 ± 0.006

Spectral and Structural Characterization throughout carbonation reaction

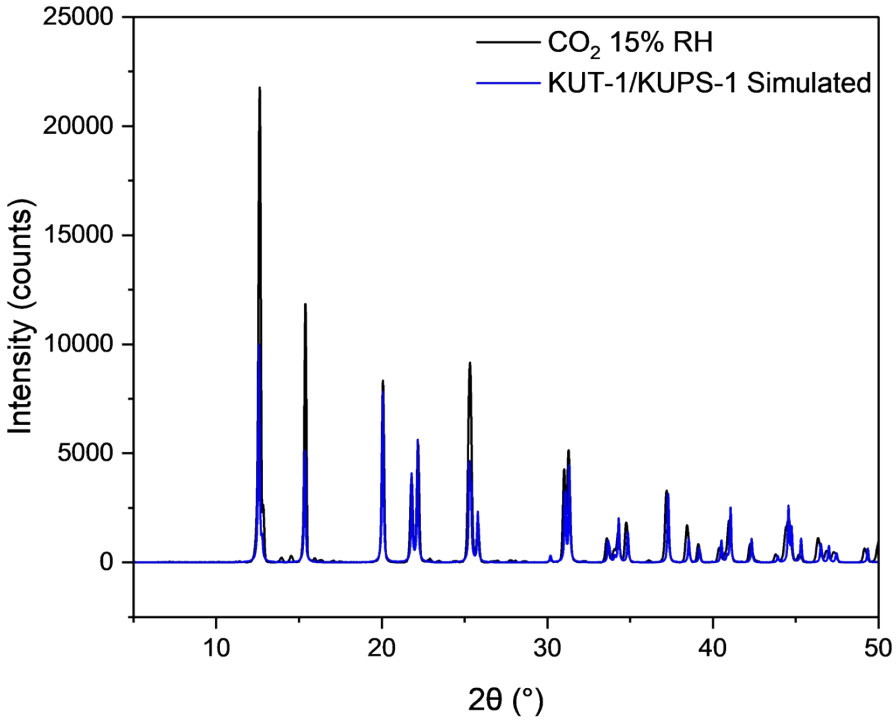

Figure S17. PXRD of KUT-1 following 2 hours of CO_2 exposure with 15% relative humidity (black) showing retention of the original material. The simulated KUT-1 pattern is shown as the blue trace.

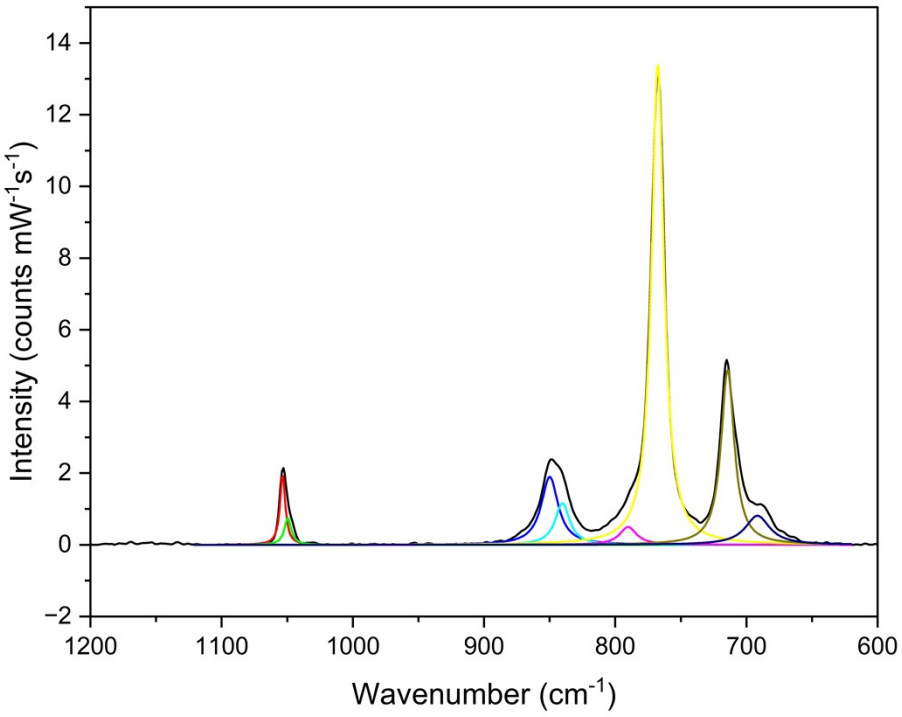

Figure S18. Fitted Raman spectrum of KUT-1 exposed to CO_2 at 45% RH for 2 hours and then aged for 3 days in a glass vial in the spectral window of interest ($\chi^2 = 0.01$; $R^2 = 0.999$).

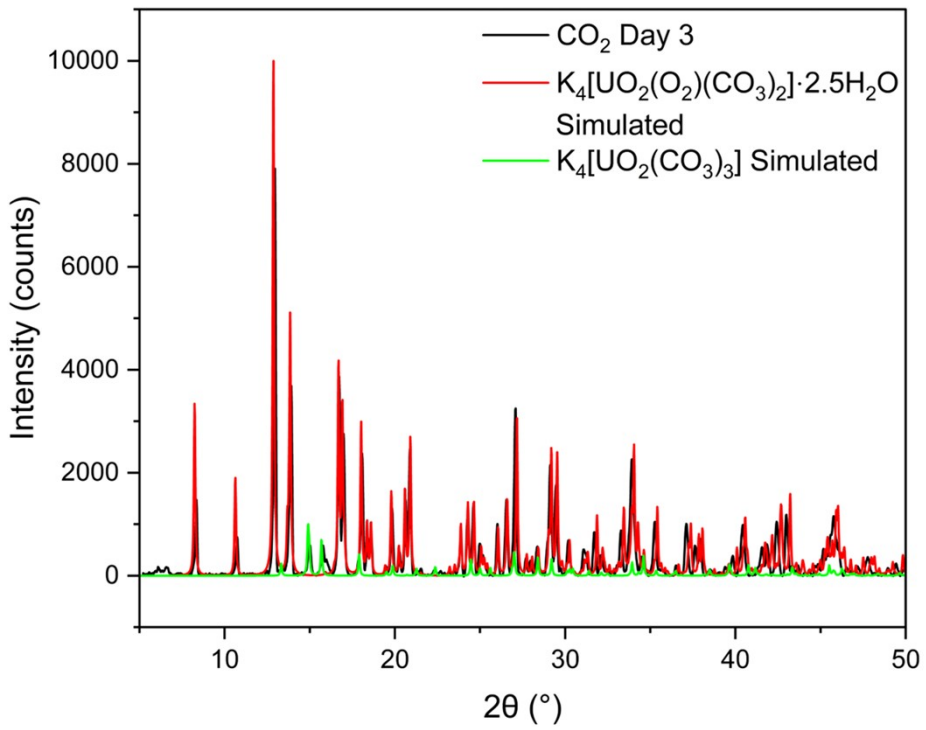

Figure S19. PXRD of KUT-1 exposed to CO_2 at 45% RH for 2 hours and then aged for 3 days in a glass vial (black) matching the simulated pattern for $K_4[UO_2(O_2)(CO_3)_2]\cdot 2.5H_2O$ (red) and $K_4[UO_2(CO_3)_3]$ (green).

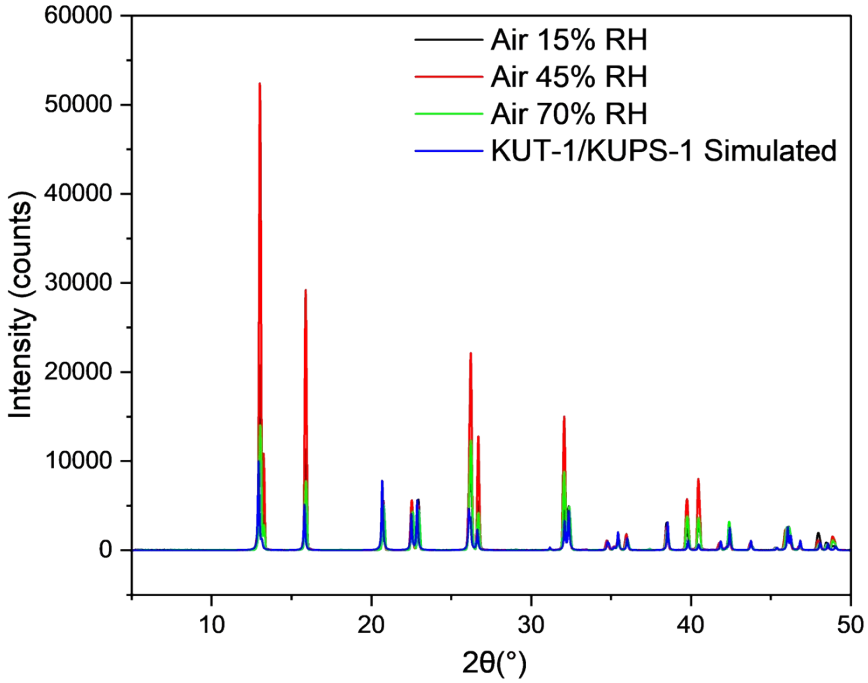

Figure S20. PXRD of the KUT-1 samples following 2 hours of air exposure at 15% (black), 45% (red) and 70% (green) relative humidity matching the simulated KUT-1 pattern (blue) and confirming no reactivity.

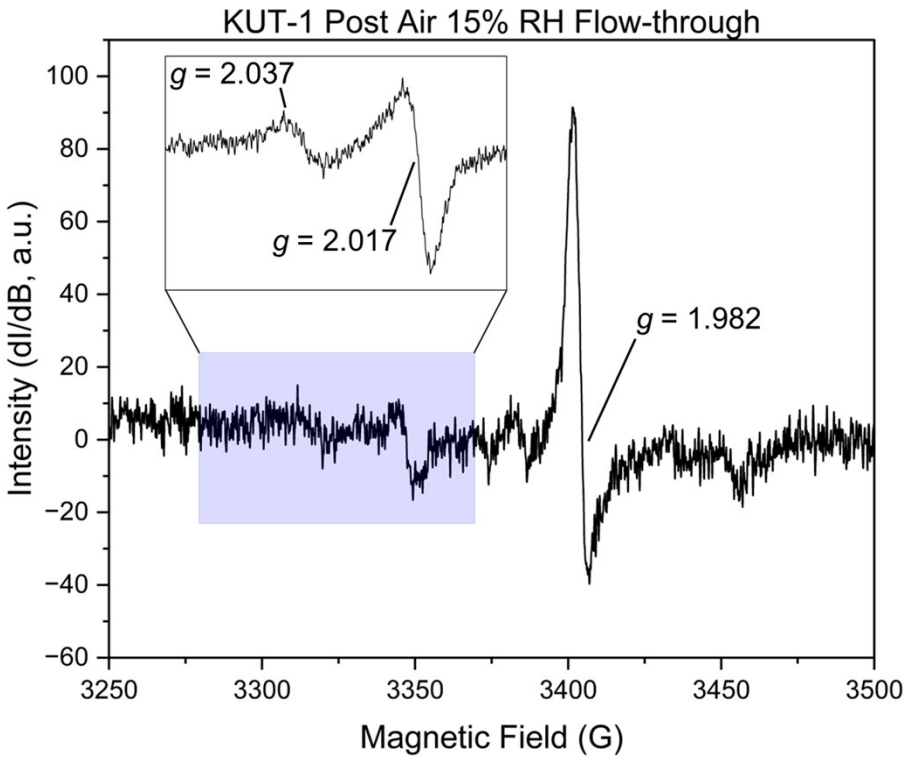

Figure S21. EPR spectrum of the KUT-1 material after air exposure with 15% relative humidity. The feature at g = 1.982 corresponds to a Cr(V) peroxide trace contaminant. Additional signatures ($g_{\parallel}$ = 2.037, $g_{\perp}$ = 2.017) corresponds to superoxide complexed to the U(VI) cation.

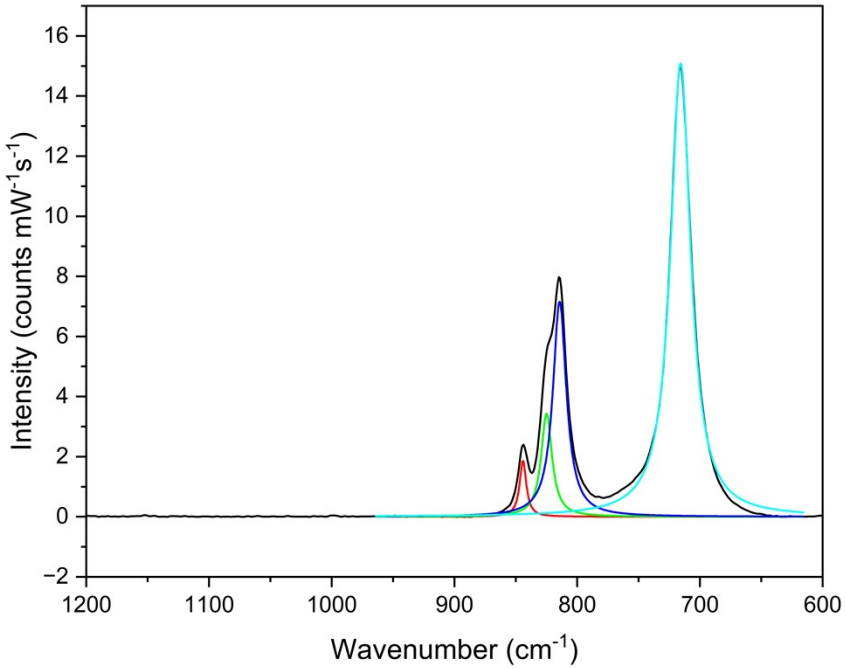

Figure S22. Fitted Raman spectrum of KUT-1 three days after exposure to compressed air (χ^2 = 0.02; R^2 = 0.999).

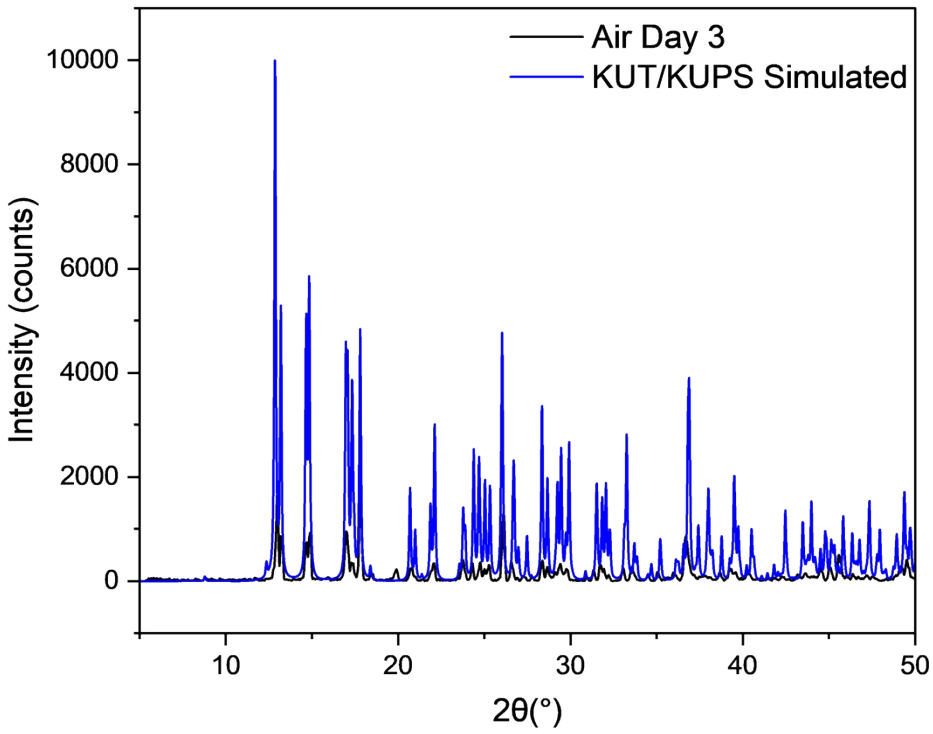

Figure S23. PXRD of the KUT-1 exposed to compressed air for 2 hours at 45% RH and then aged for 3 days (black) under ambient conditions showing conversion to KUT (simulated pattern in blue).

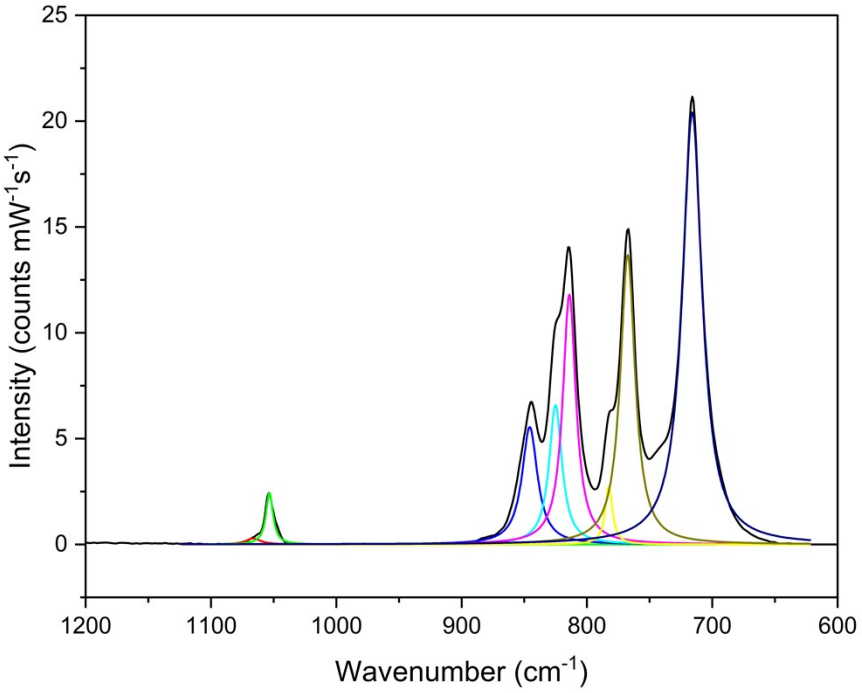

Figure S24. Raman fitting parameters for KUT-1 6 days after the exposure to compressed air for 2 hours at 15% RH experiment. Bands are located at 1066, 1053, 846, 814, 783, 768, and 716 cm^{-1} ($\chi^2 = 0.06$; $R^2 = 0.999$).

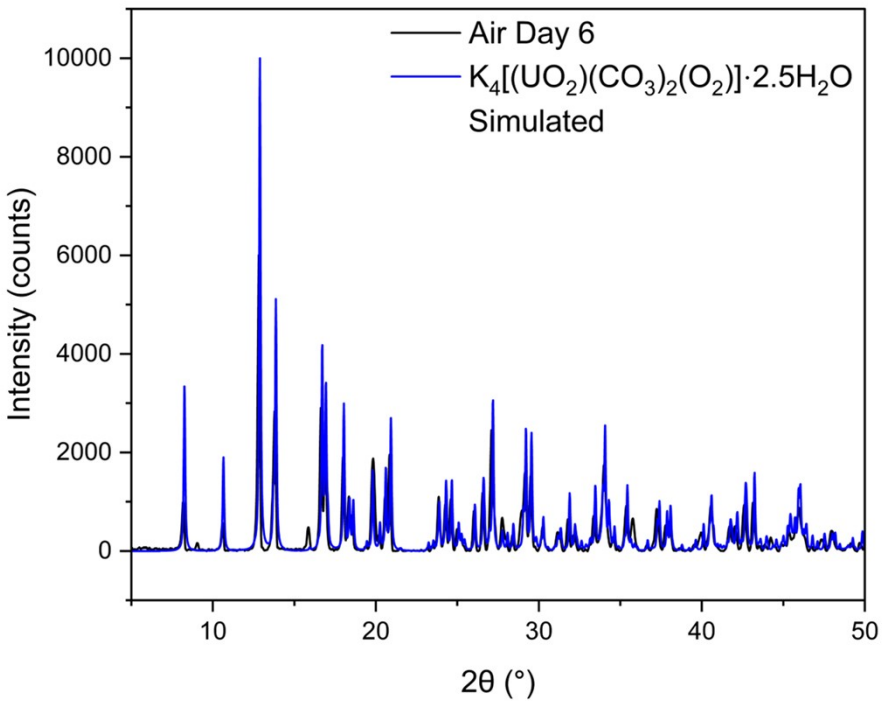

Figure S25. PXRD of the KUT-1 exposed to compressed air for 2 hours at 15% RH and then aged for 6 days (black) under ambient conditions showing further conversion from KUT (Fig. S21) to the potassium uranyl peroxo-carbonate phase (simulated pattern in blue).

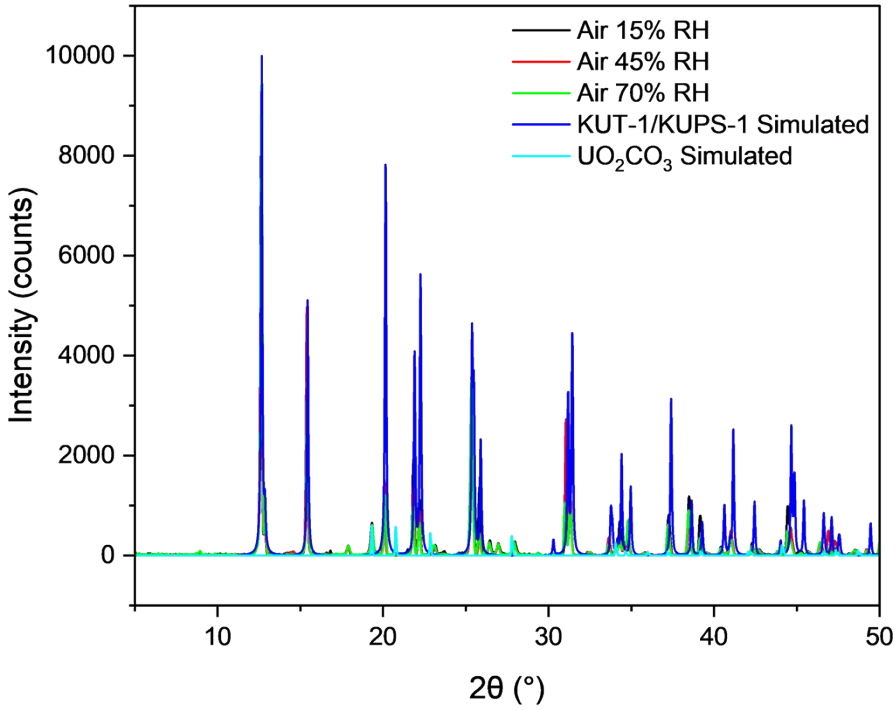

Figure S26. PXRD of the KUPS-1 samples following 2 hours of air exposure at 15% (black), 45% (red) and 70% (green) relative humidity matching the simulated KUPS-1 pattern (blue) and UO_2CO_3 (teal).

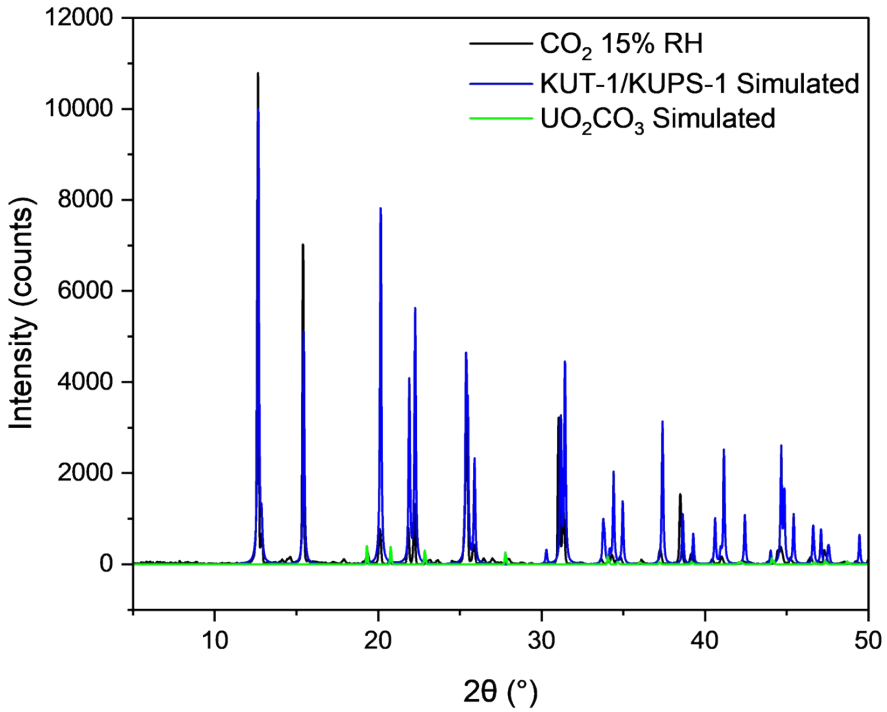

Figure S27. PXRD of KUPS-1 following 2 hours of CO_2 exposure with 15% relative humidity (black) showing retention of the KUPS-1 phase with the simulated KUPS-1 pattern in blue, in addition to new smaller features matching with the simulated UO_2CO_3 pattern (green).

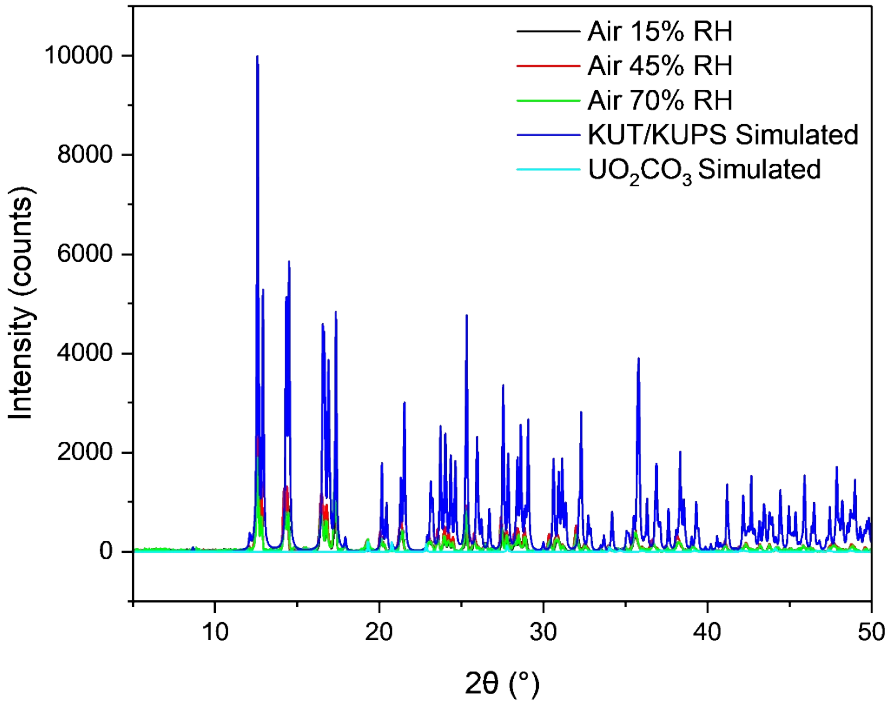

Figure S28. PXRD of the KUT samples following 2 hours of air exposure at 15% (black), 45% (red) and 70% (green) relative humidity matching the simulated KUT pattern (blue) and the simulated UO_2CO_3 (Rutherfordine) pattern (teal).

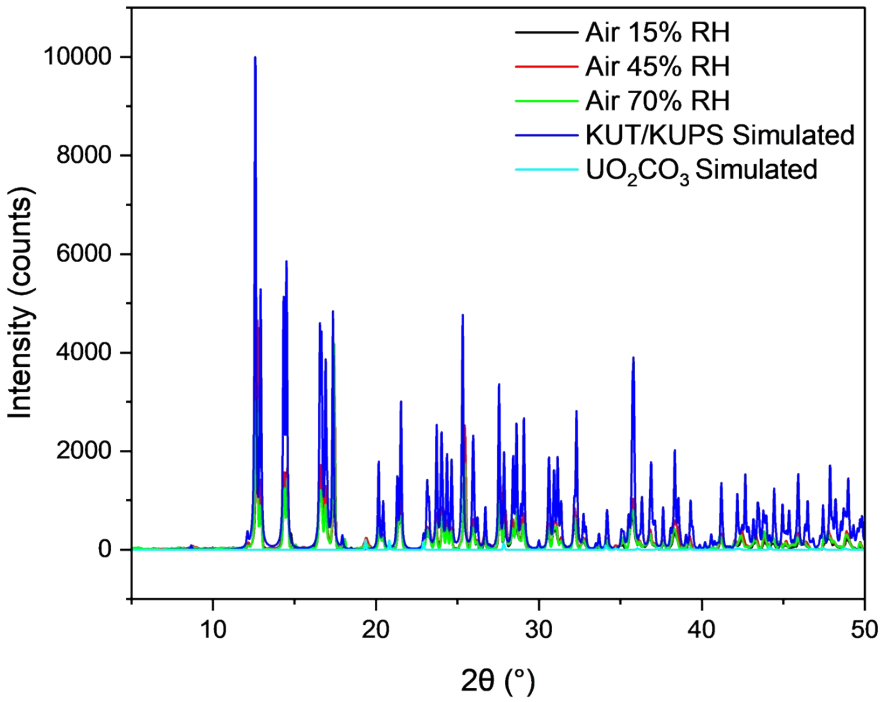

Figure S29. PXRD of the KUPS samples following 2 hours of air exposure at 15% (black), 45% (red) and 70% (green) relative humidity matching the simulated KUPS pattern (blue) and the simulated UO_2CO_3 (Rutherfordine) pattern (teal).

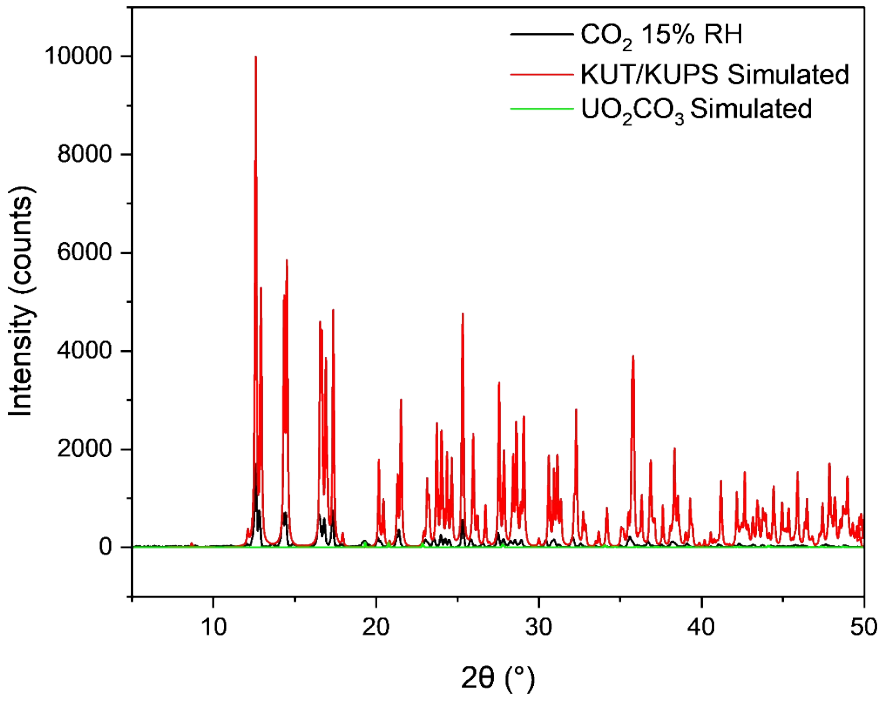

Figure S30. PXRD of KUT following 2 hours of CO_2 exposure with 15% relative humidity (black), the simulated KUT pattern (red) and the simulated UO_2CO_3 (Rutherfordine) pattern (green).

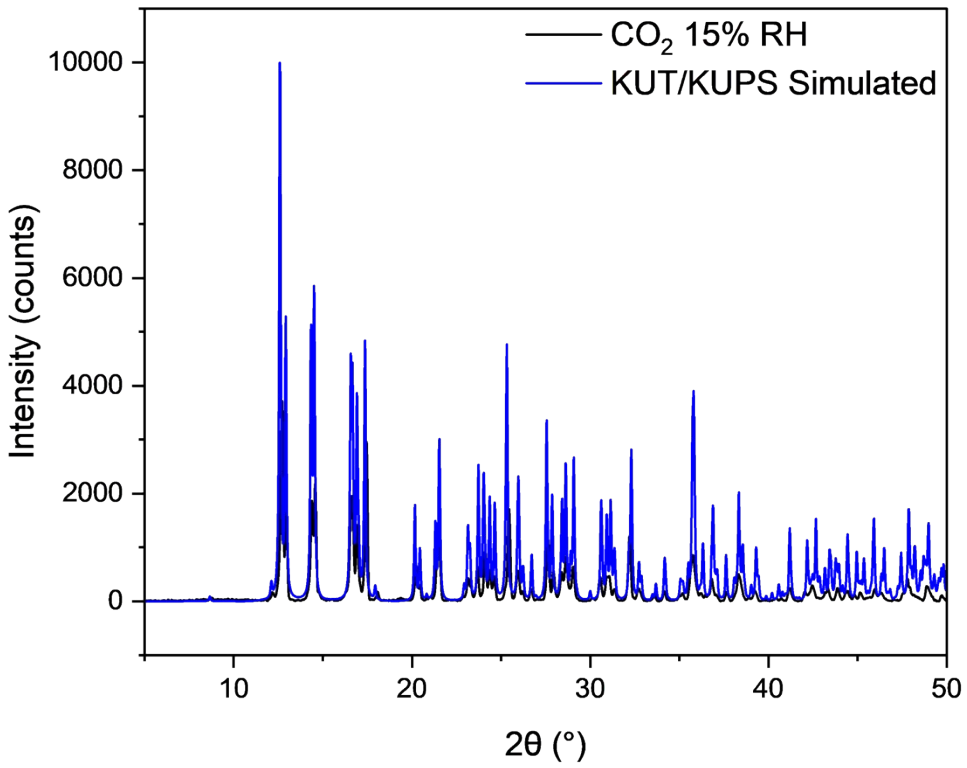

Figure S31. PXRD of KUPS following 2 hours of CO_2 exposure with 15% relative humidity (black) showing retention of the KUPS phase with the simulated KUPS pattern in blue.

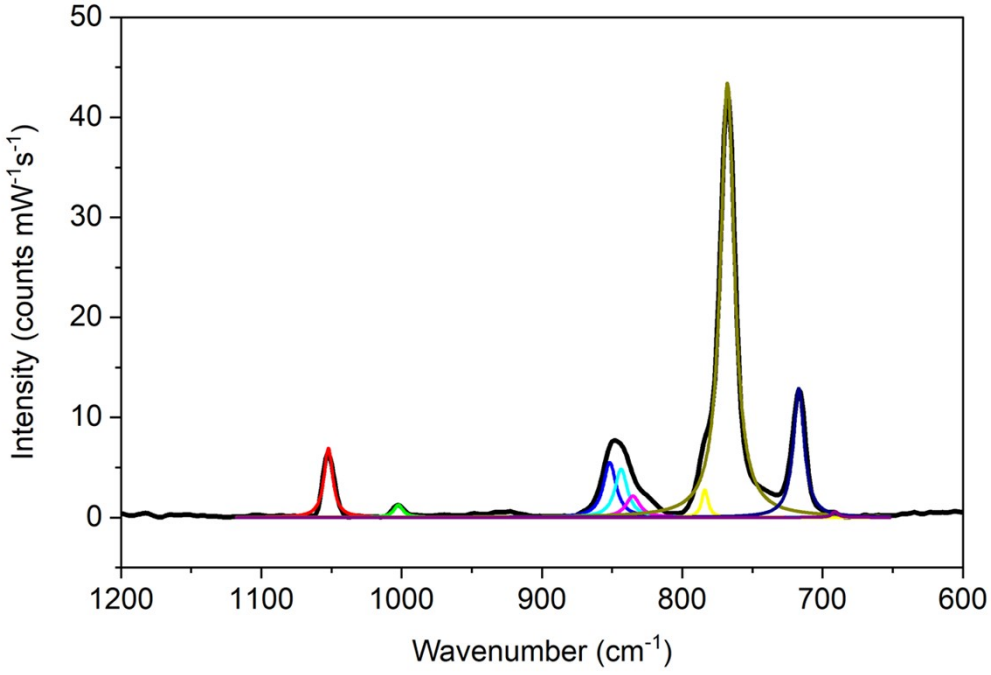

Figure S32. Raman Spectrum of KUT-1 exposed to ambient laboratory air for 24 hours, demonstrating carbonation with band at 1052 cm^{-1} ($\chi^2 = 0.23$; $R^2 = 0.994$).

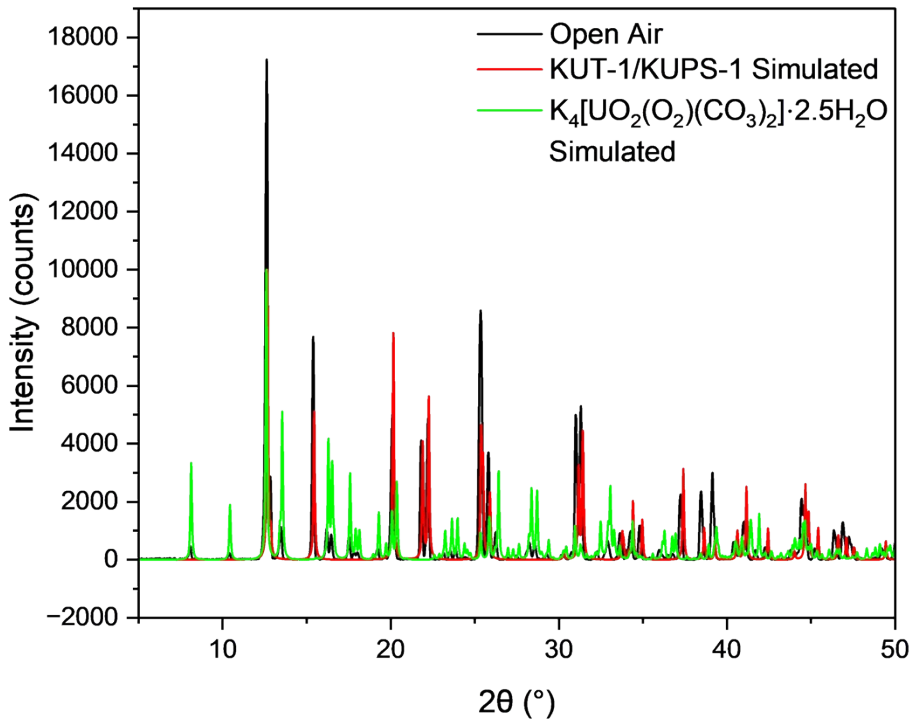

Figure S33. PXRD of the KUT-1 sample exposed to open air for 1 day (black), simulated KUT-1 (red) and simulated potassium uranyl peroxo-carbonate (green).

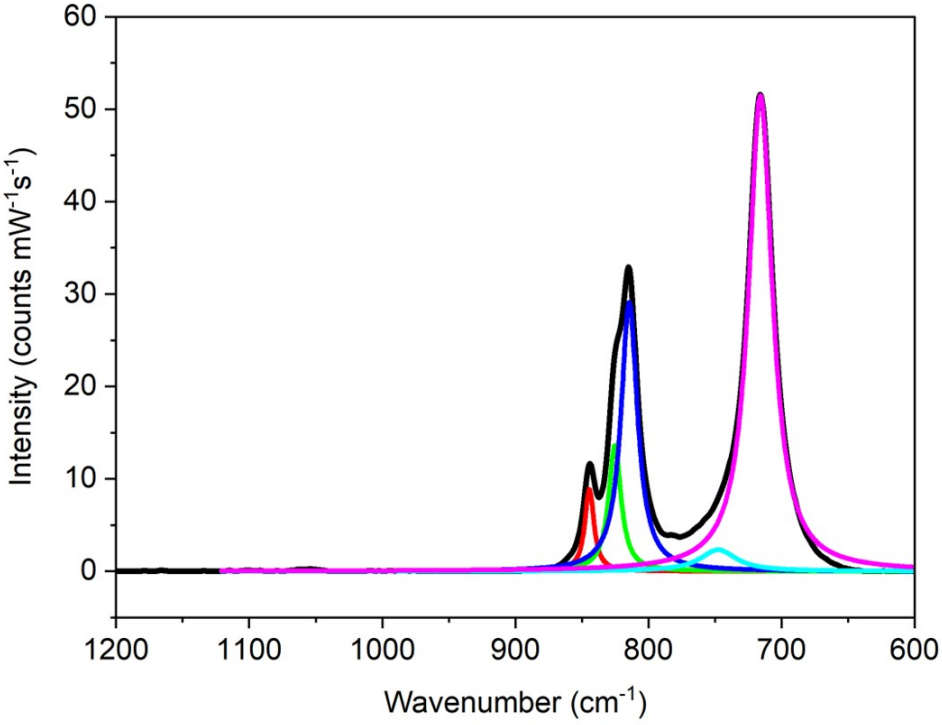

Figure S34. Raman Spectrum of KUT-1 exposed to a continuous flow of air for 24 hours, demonstrating decomposition of lattice H_2O_2 and conversion to KUT ($\chi^2 = 0.26$; $R^2 = 0.998$).

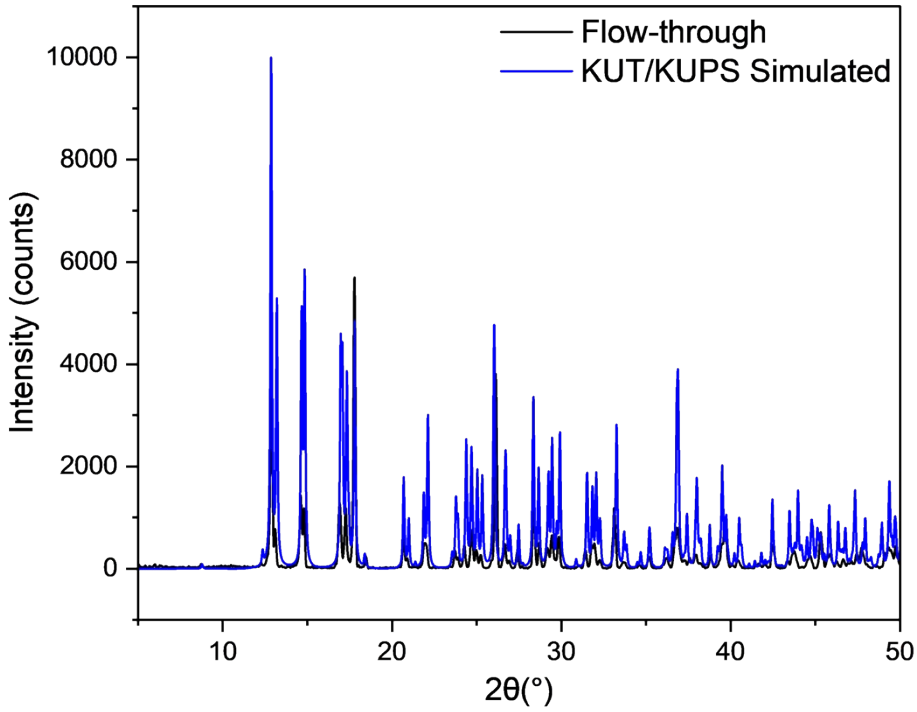

Figure S35. PXRD of the KUT-1 sample exposed to a continuous flow of air for 24 hours (black), demonstrating decomposition of lattice H_2O_2 and conversion to KUT (simulated pattern in blue).

Carbonation Reaction Kinetic Modelling

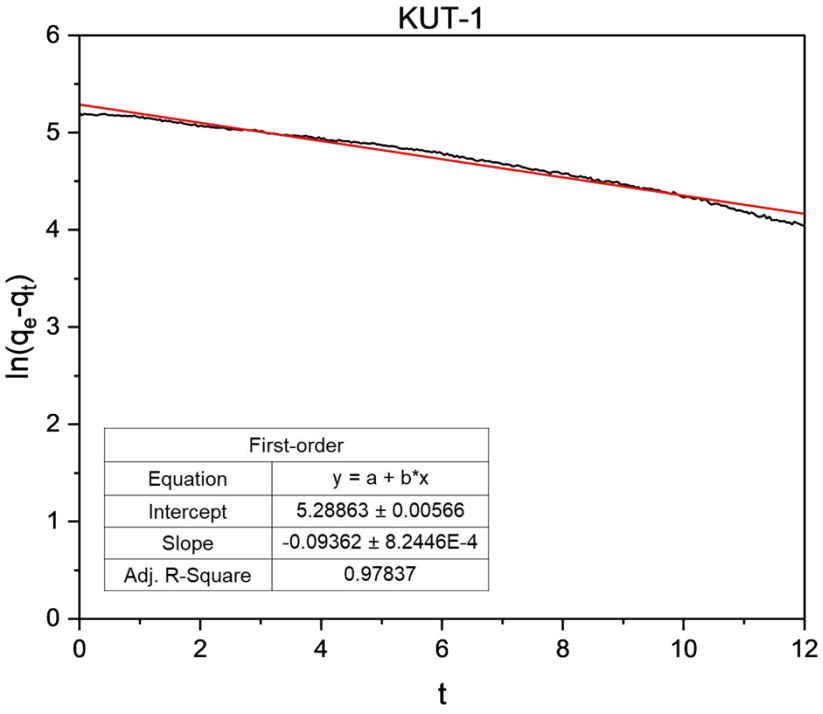

Figure S36. First-order modelling of the carbonation kinetics for KUT-1 where t is time in days, q_e is the equilibrium CO_2 concentration in ppm and q_t is the CO_2 concentration in ppm at time t.

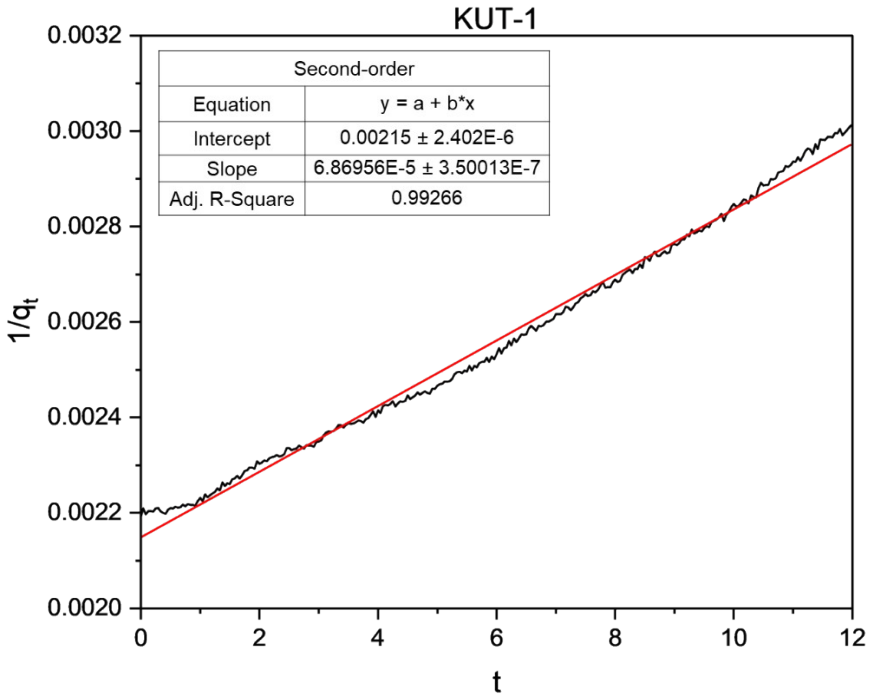

Figure S37. Second-order modelling of the carbonation kinetics for KUT-1 where t is time in days and q_t is the CO_2 concentration in ppm at time t.

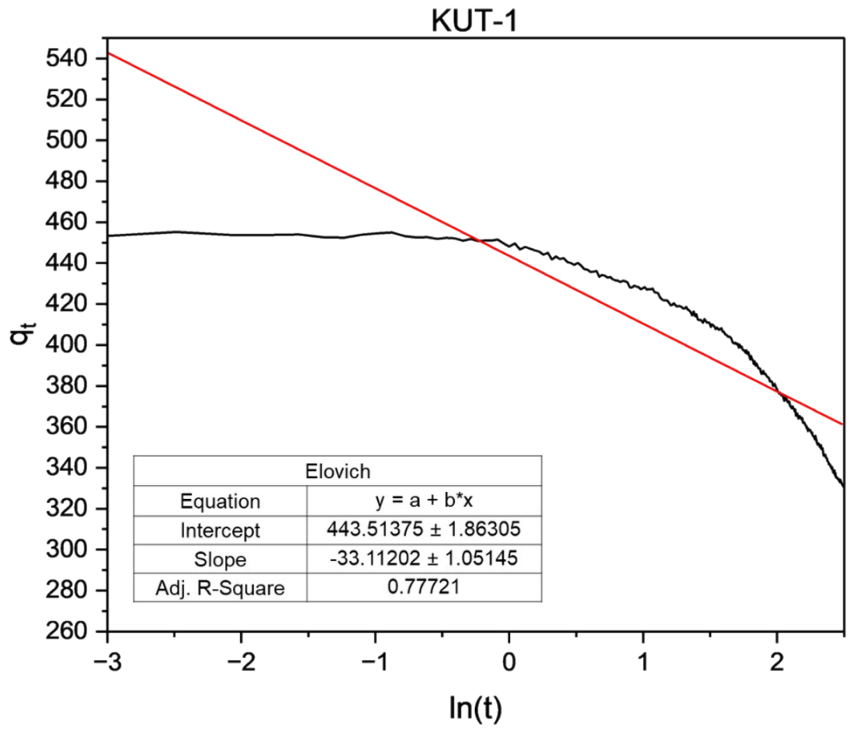

Figure S38. Elovich modelling of the carbonation kinetics for KUT-1 where t is time in days and q_t is the CO_2 concentration in ppm at time t.

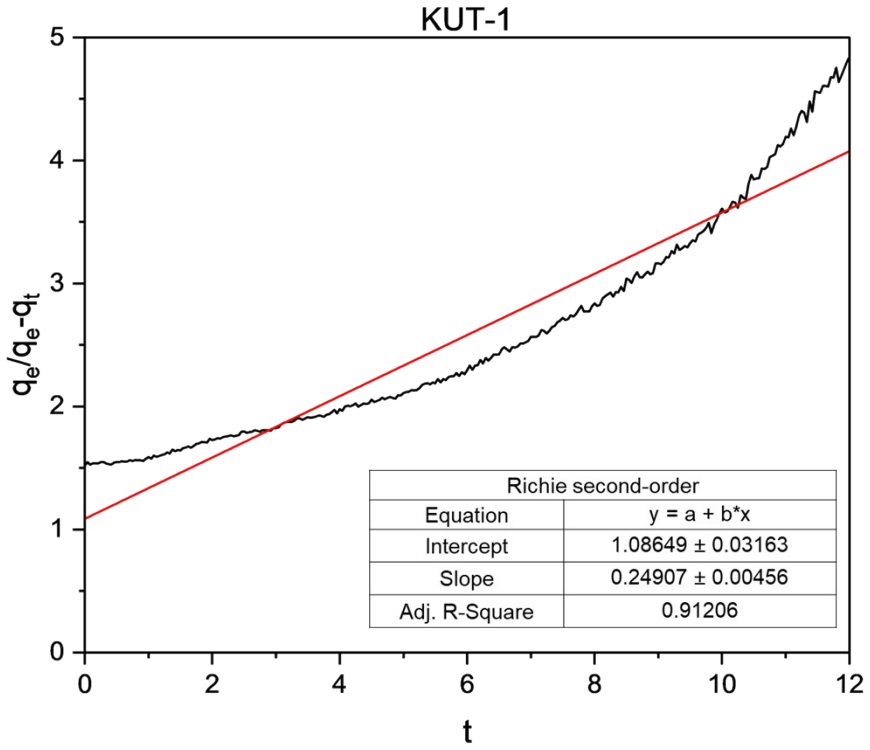

Figure S39. Richie second-order modelling of the carbonation kinetics for KUT-1 where t is time in days, q_e is the equilibrium CO_2 concentration in ppm and q_t is the CO_2 concentration in ppm at time t.

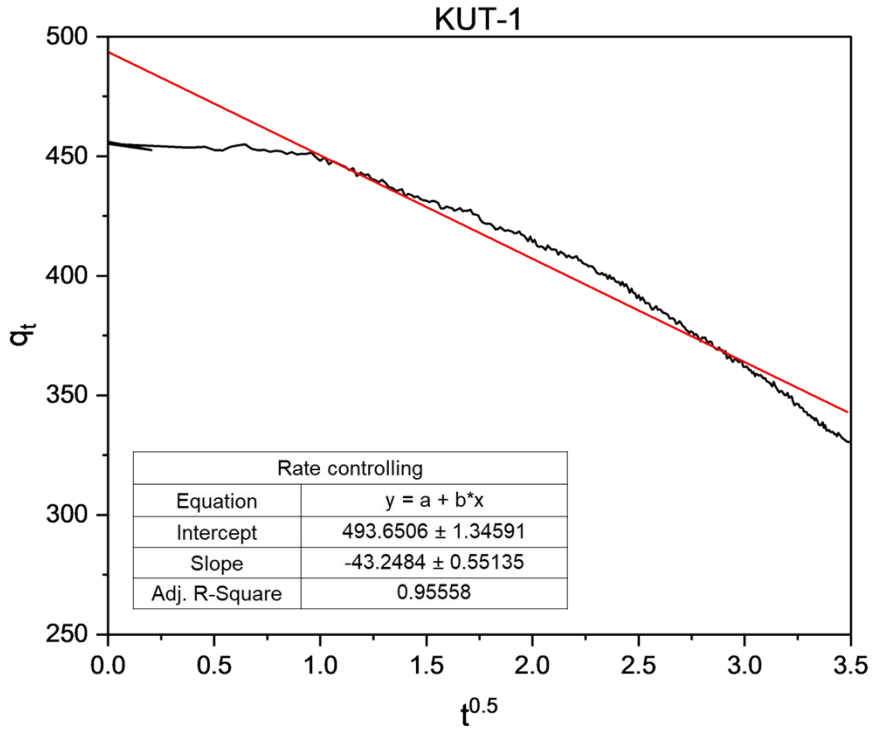

Figure S40. Rate controlling modelling of the carbonation kinetics for KUT-1 where t is time in days and q_t is the CO_2 concentration in ppm at time t.

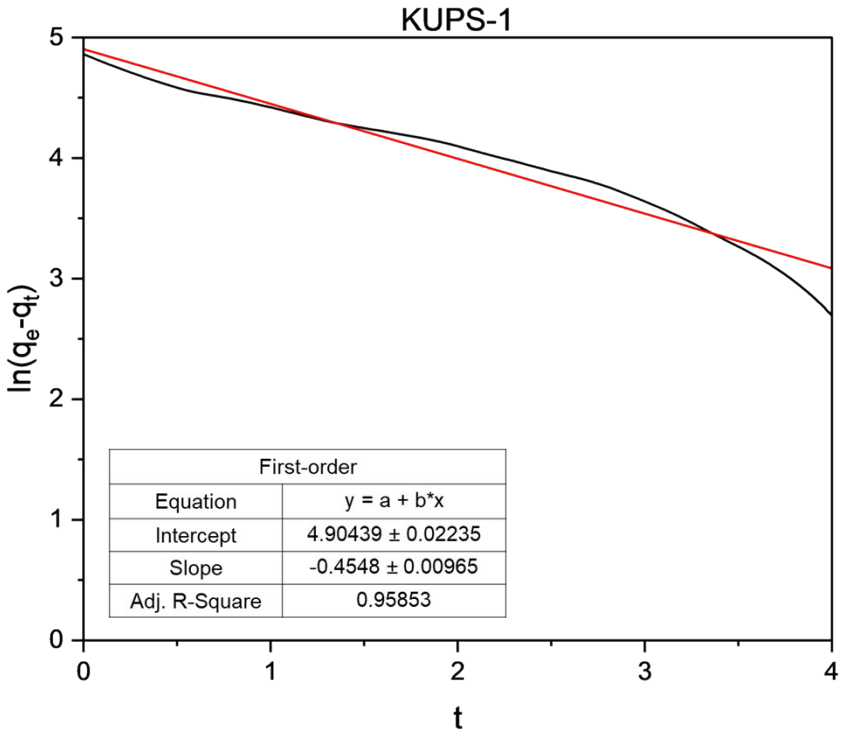

Figure S41. First-order modelling of the carbonation kinetics for KUPS-1 where t is time in days, q_e is the equilibrium CO_2 concentration in ppm and q_t is the CO_2 concentration in ppm at time t.

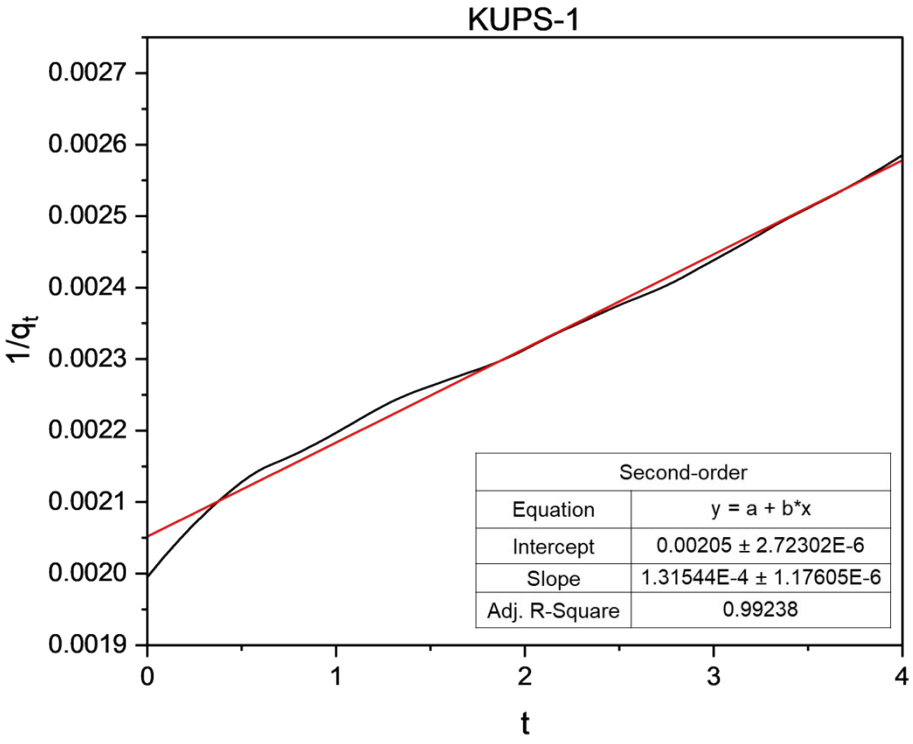

Figure S42. Second-order modelling of the carbonation kinetics for KUPS-1 where t is time in days and q_t is the CO_2 concentration in ppm at time t.

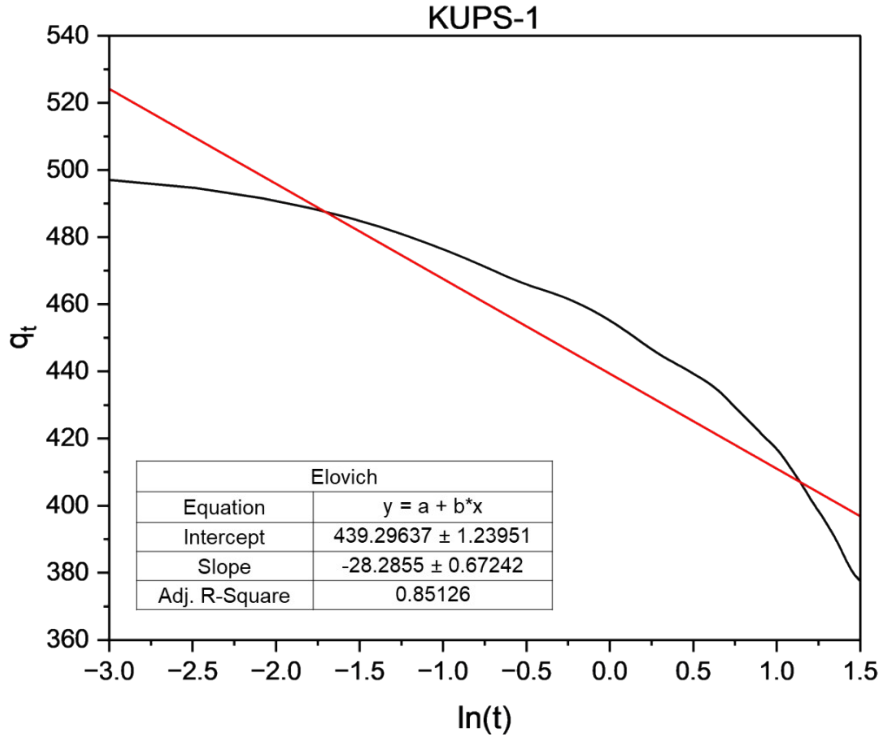

Figure S43. Elovich modelling of the carbonation kinetics for KUPS-1 where t is time in days and q_t is the CO_2 concentration in ppm at time t.

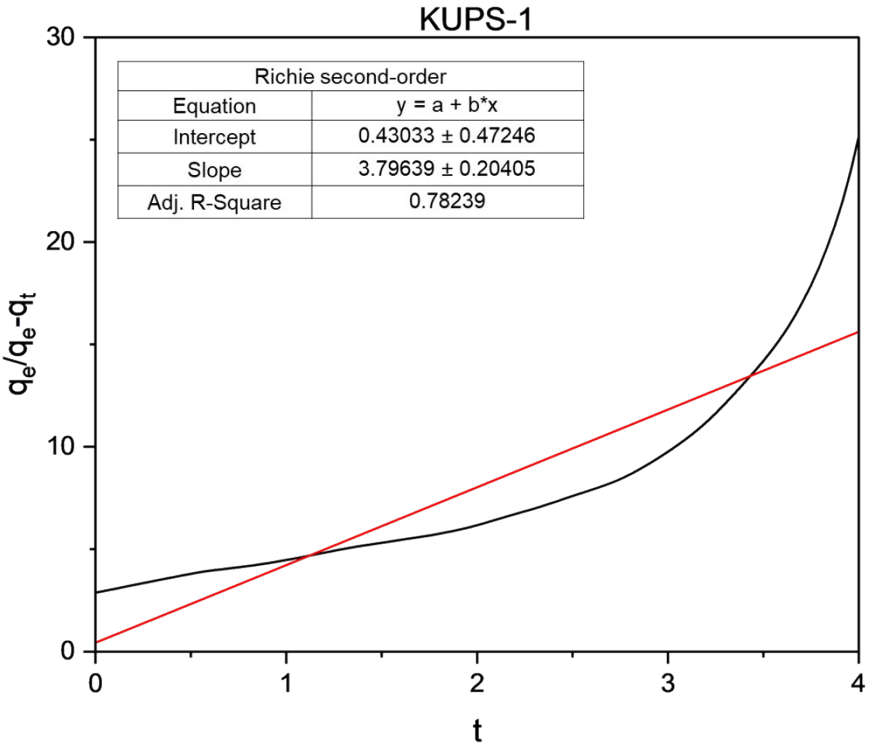

Figure S44. Richie second-order modelling of the carbonation kinetics for KUPS-1 where t is time in days, q_e is the equilibrium CO_2 concentration in ppm and q_t is the CO_2 concentration in ppm at time t.

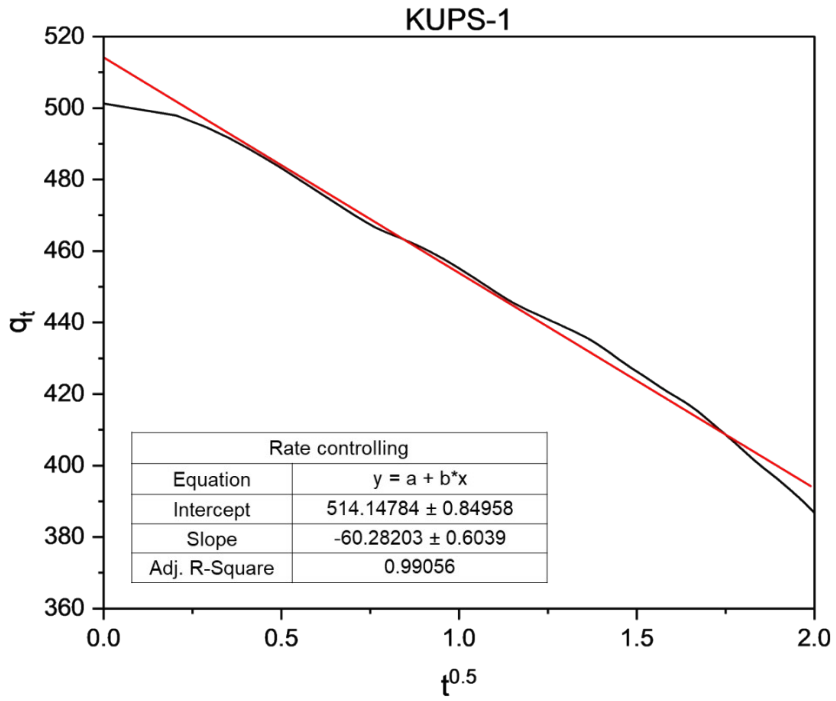

Figure S45. Rate controlling modelling of the carbonation kinetics for KUPS-1 where t is time in days and q_t is the CO_2 concentration in ppm at time t.

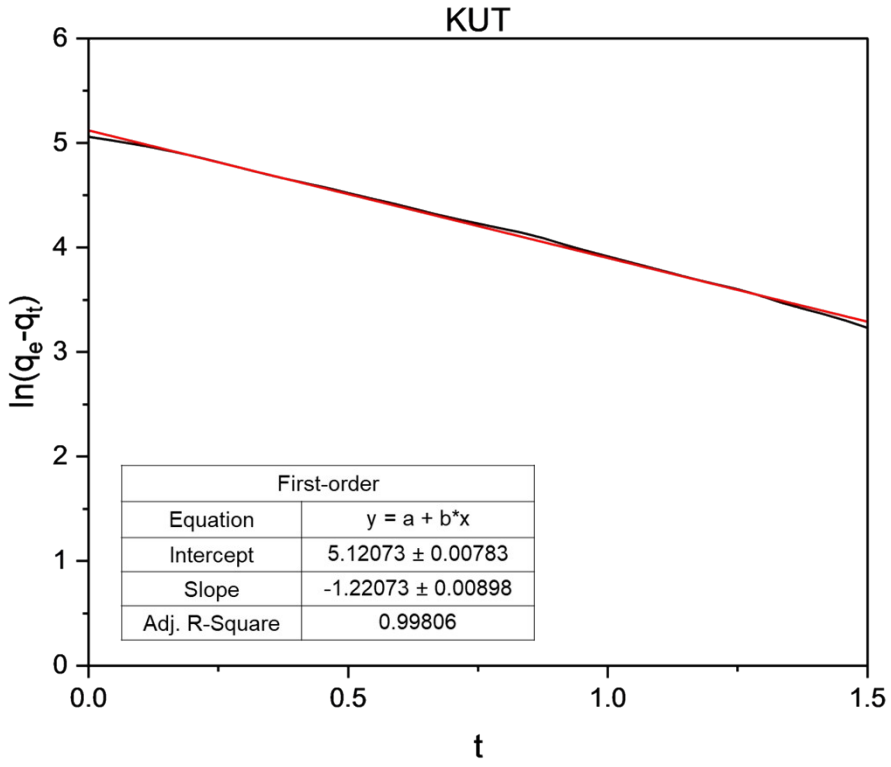

Figure S46. First-order modelling of the carbonation kinetics for KUT where t is time in days, q_e is the equilibrium CO_2 concentration in ppm and q_t is the CO_2 concentration in ppm at time t.

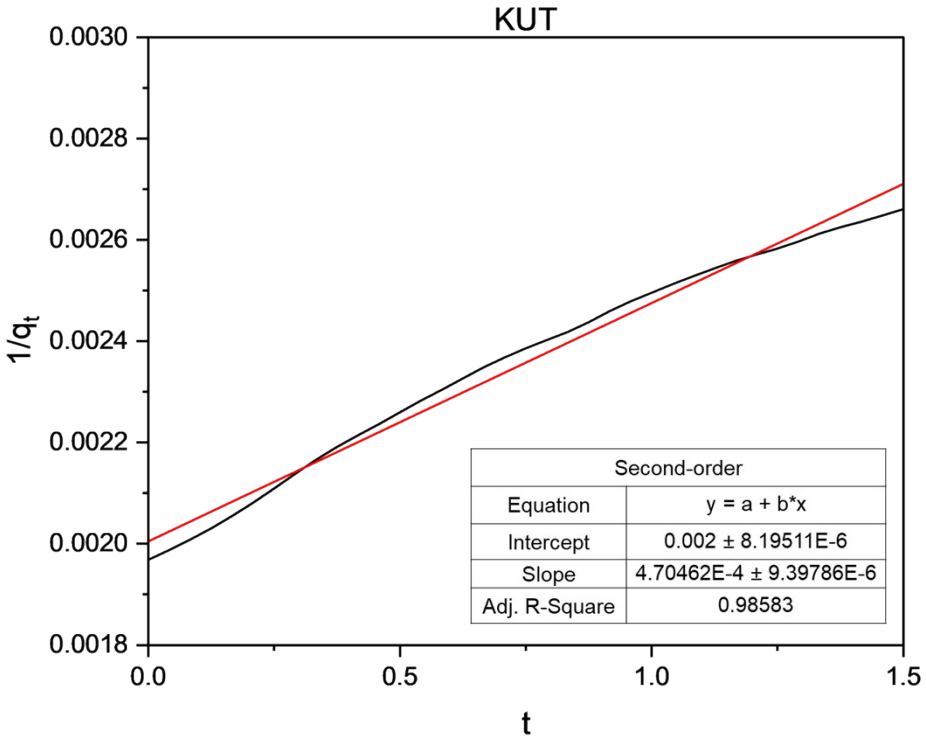

Figure S47. Second-order modelling of the carbonation kinetics for KUT where t is time in days and q_t is the CO_2 concentration in ppm at time t.

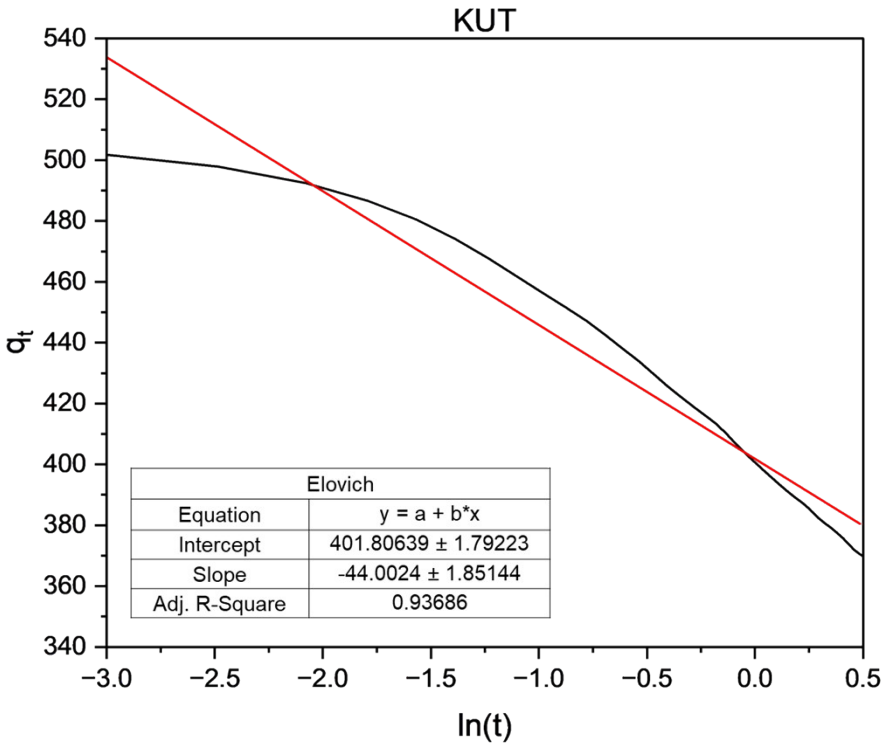

Figure S48. Elovich modelling of the carbonation kinetics for KUT where t is time in days and q_t is the CO_2 concentration in ppm at time t.

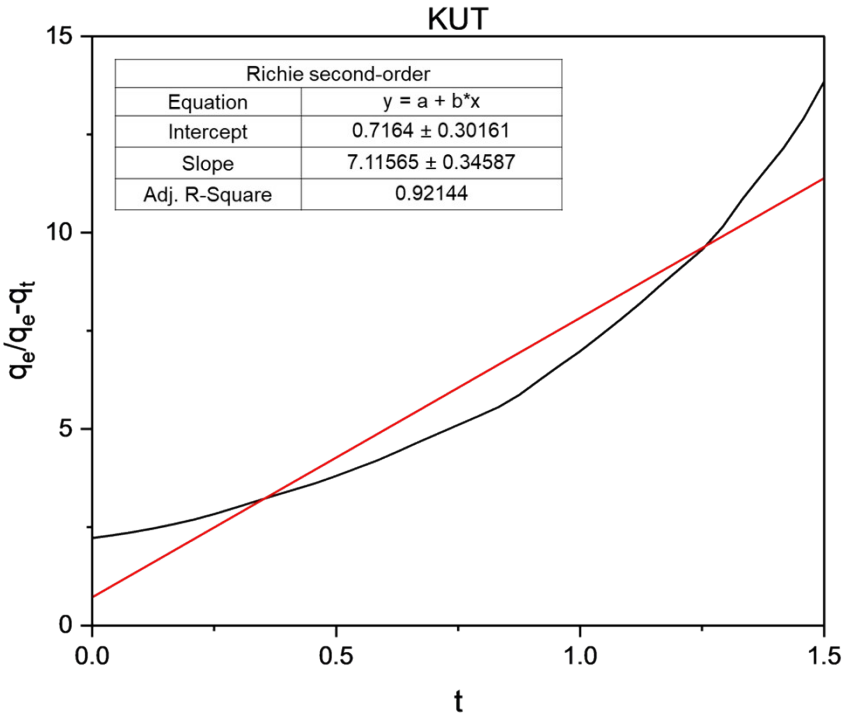

Figure S49. Richie second-order modelling of the carbonation kinetics for KUT where t is time in days, q_e is the equilibrium CO_2 concentration in ppm and q_t is the CO_2 concentration in ppm at time t.

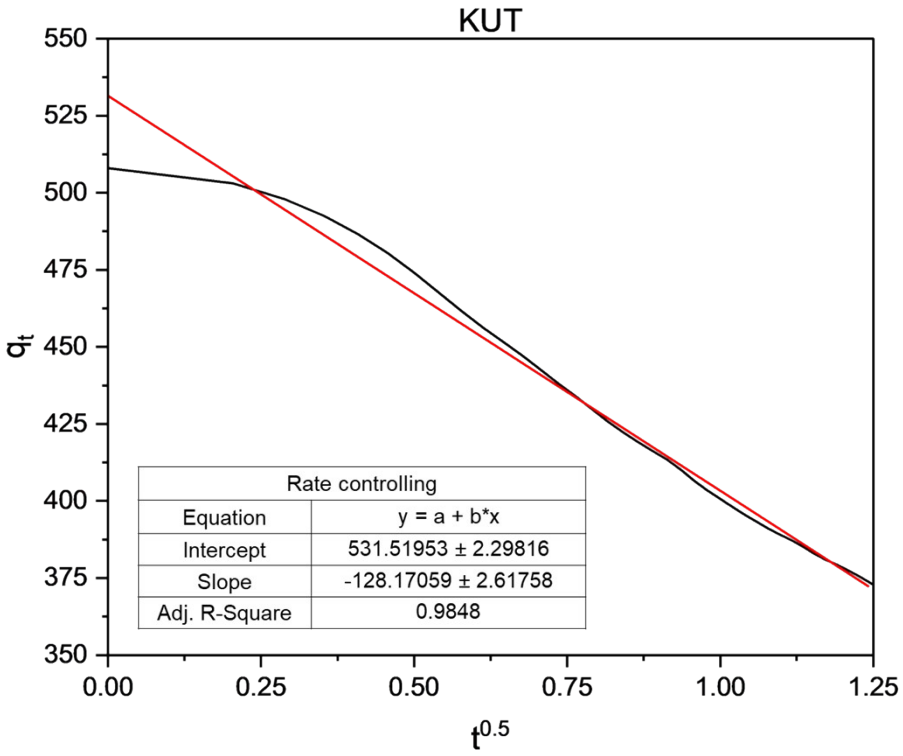

Figure S50. Rate controlling modelling of the carbonation kinetics for KUT where t is time in days and q_t is the CO_2 concentration in ppm at time t.

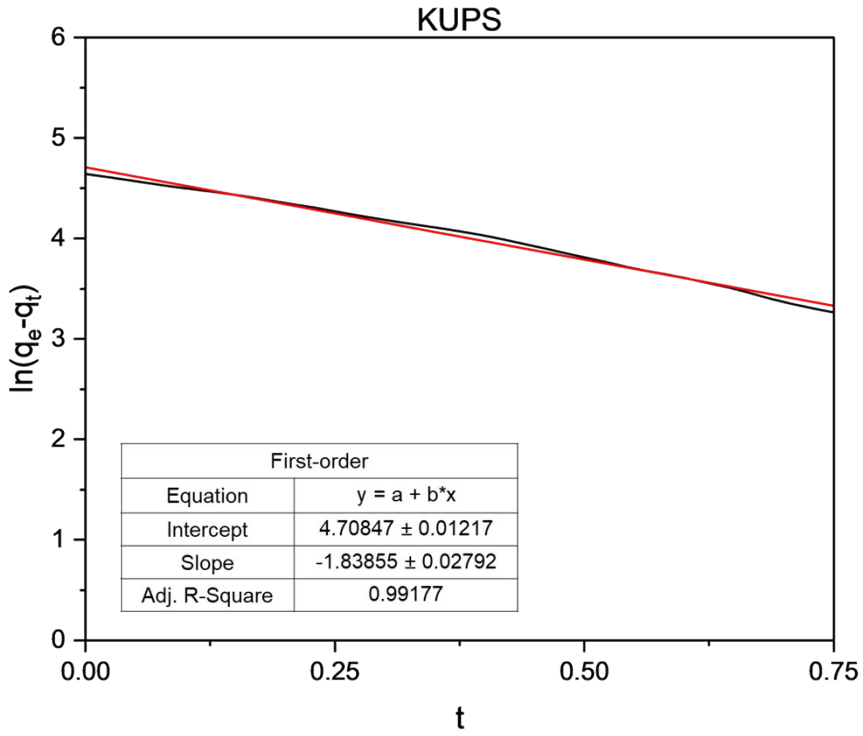

Figure S51. First-order modelling of the carbonation kinetics for KUPS where t is time in days, q_e is the equilibrium CO_2 concentration in ppm and q_t is the CO_2 concentration in ppm at time t.

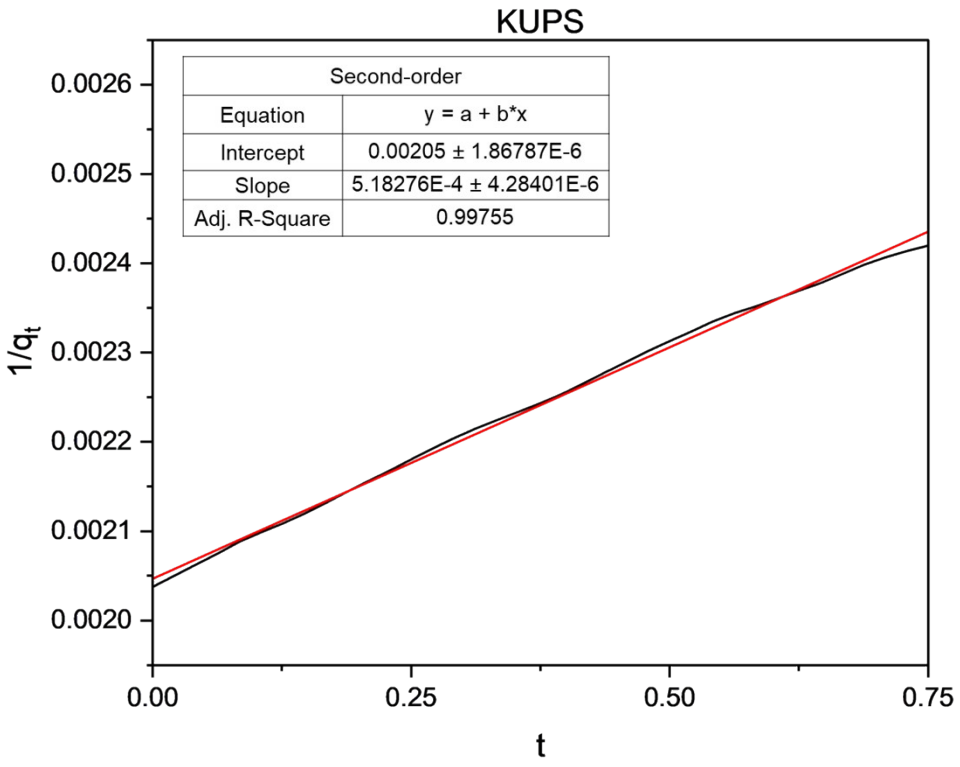

Figure S52. Second-order modelling of the carbonation kinetics for KUPS where t is time in days and q_t is the CO_2 concentration in ppm at time t.

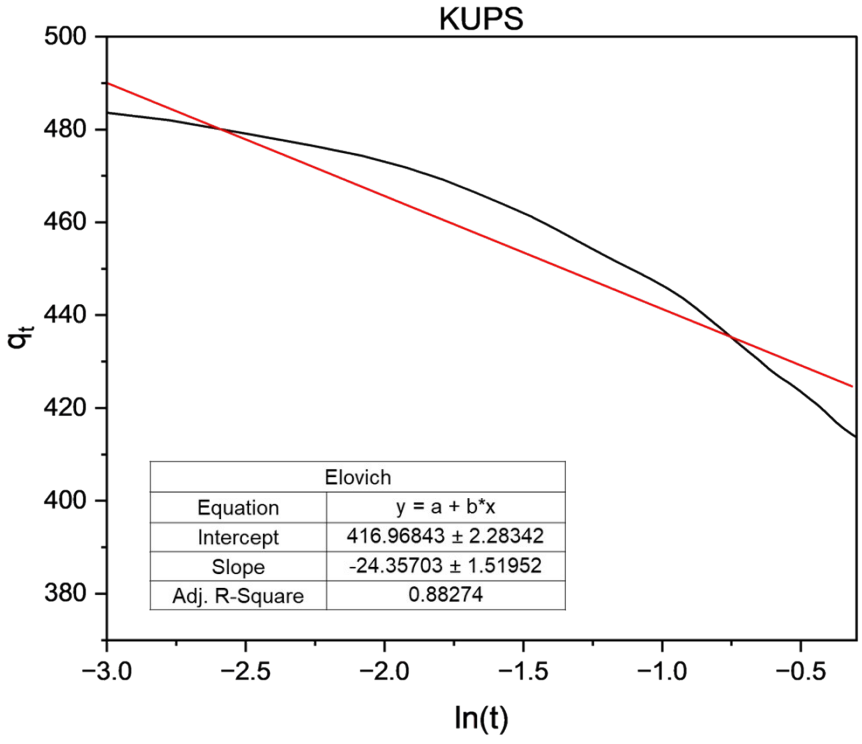

Figure S53. Elovich modelling of the carbonation kinetics for KUPS where t is time in days and q_t is the CO_2 concentration in ppm at time t.

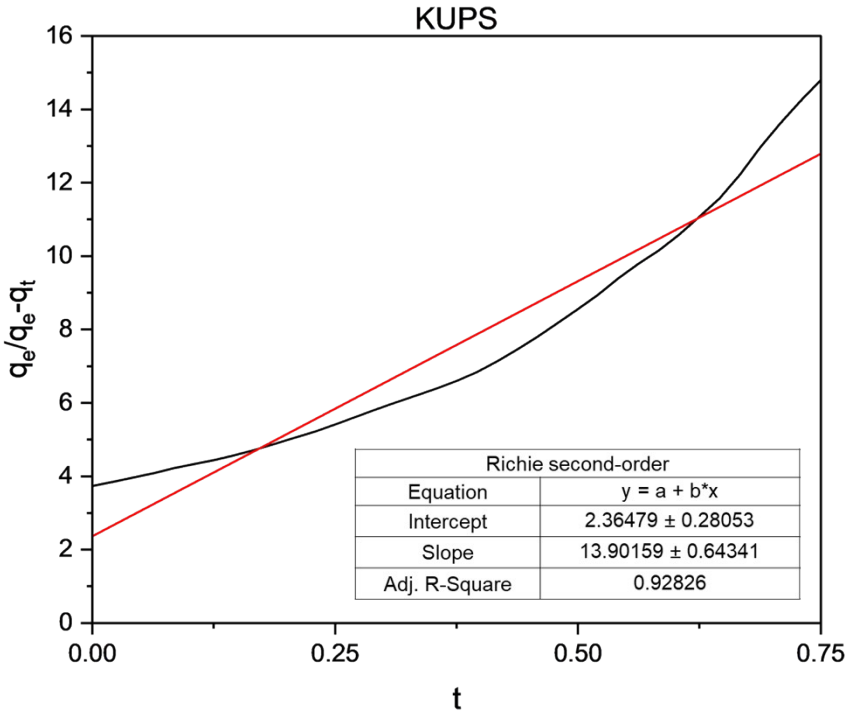

Figure S54. Richie second-order modelling of the carbonation kinetics for KUPS where t is time in days, q_e is the equilibrium CO_2 concentration in ppm and q_t is the CO_2 concentration in ppm at time t.

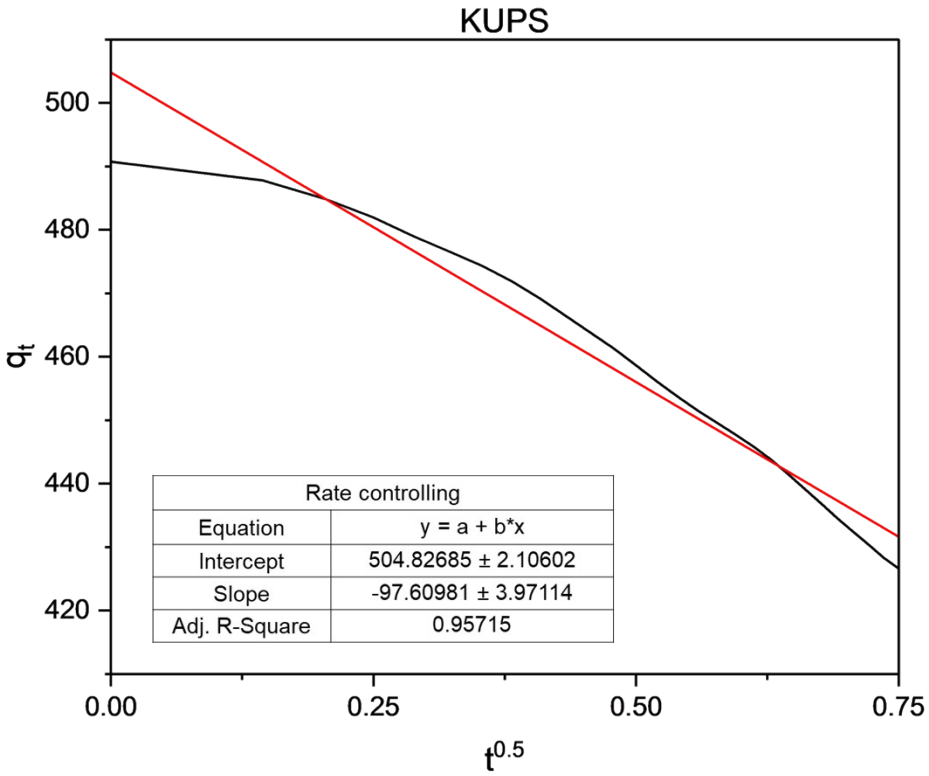

Figure S55. Rate controlling modelling of the carbonation kinetics for KUPS where t is time in days and q_t is the CO_2 concentration in ppm at time t.